LOW CARBON ULTRAFINE GRAINED DUAL PHASE STEELS

by

VISHNU CHARAN SANGEM

B.Tech (Hons), Indian Institute of Technology (IIT), 2009

A THESIS SUBMITTED IN PARTIAL FULFILLMENT OF THE REQUIREMENTS FOR

THE DEGREE OF

MASTER OF APPLIED SCIENCE

in

THE FACULTY OF GRADUATE STUDIES
(Materials Engineering)

THE UNIVERSITY OF BRITISH COLUMBIA
(Vancouver)

May 2012

Abstact

Ultrafine grained (UFG) (i.e. grain size of the order 1 μm) dual phase (DP) steels have been investigated using a thermo-mechanical process designed to obtain fine ferrite-carbide aggregates prior to intercritical annealing. The effects of carbon content, alloying additions, initial starting structures and processing parameters like heating and cooling rate on the mechanical properties have been quantified. Experimental work was conducted on two plain low carbon steels (0.06 and 0.12 wt pct C) and two low carbon (0.06 wt pct) micro-alloyed steels, one with Mo (0.15 wt pct) and the other with Nb (0.06 wt pct) addition, respectively.

Fine ferrite-carbide aggregates were obtained only for the plain carbon steels and not for the micro-alloyed steels; hence no further studies are carried out for the micro-alloyed steels. A Gleeble 3500 thermomechanical simulator is used for the intercritical annealing operation to obtain UFG DP steels. The tensile test results showed that a critical carbon (about 0.1 wt pct) content may be necessary for obtaining a good balance of strength and ductility. The lower carbon steels showed better true strain to fracture behavior, but fall behind in terms of strength and ductility compared to the higher carbon steel. Higher heating rates are necessary for achieving fine microstructures as well as better mechanical properties, whereas lower heating rates helped in obtaining good strength-elongation (engineering tensile strength × uniform elongation) balance.

For the sake of comparison martensite starting structures are also used to obtain UFG DP steels. There is no effect of heating rate on the strength values, but higher heating rates resulted in better elongation as well as fracture strain values. Overall, the UFG DP steels fabricated by using

martensite starting structures showed better strength-elongation balance, moreover the number of processing steps are considerably reduced.

Table of Contents

List of Tables

List of Figures

Acknowledgements

I would like to take this opportunity to express my utmost gratitude towards my supervisor Dr. Matthias Militzer for giving me the freedom both on academic as well as personal front. I would also like to thank Dr. Hamid Azizi-Alizamini, who has been a great mentor and guide right from my undergraduate days. I have learnt a lot from both of them over the past two years, especially from the time I started writing my thesis. I am grateful to them and I selfishly expect to have their support and advice in the future as well.

I would like to thank Ross McLeod, Carl Ng and David Torok for preparing tons of samples and also for their humorous conversations. My conversations with Rudy Cardeno and Dr. Ainul Akhtar helped me to understand technical details of the equipment that I used, and I am immensely grateful for them. Fruitful conversations with fellow student Sina Shahandeh has helped me to focus on my research work. I would also like to thank Dr. Fateh Fazeli, for his patience in dealing with the mistakes I committed while using the Gleeble machine. AUTO 21 research network is greatly acknowledged for financial support.

I would like to thank the friends I made in this beautiful city of Vancouver for their love and encouragement. Finally, last but the most important ones, my mom and dad for their everlasting love and understanding.

1 Introduction

The demand to produce automobiles which fulfill the requirements like, passenger safety, vehicle performance and fuel efficiency, has been the biggest challenge faced by the steel industry for the last couple of decades [1, 2]. In response the steel industry has developed advanced high strength steels (AHSS) including dual phase (DP), transformation induced plasticity (TRIP), complex phase (CP) and martensitic steels (MART). These steels are characterised by improved formability and crash worthiness compared to conventional steel grades, such as pearlitic steels. Currently, AHSS steels are extensively used in the auto industry and the projections are that the weight percentage of AHSS steel will increase to 35% by 2015, whereas mild steel will decrease from 55% (in 2007) to 29% in bodies and closures of light vehicles [3]. The rationales for increased use of the AHSS in the automotive industry are as follows: (1) the reduction of the car weight resulting from the use of high strength thinner gauge sheet steel, reducing the fuel consumption; (2) Increased passenger safety by an improved crash worthiness; (3) The strong competition from the light-weight materials, such as Al and Mg alloys and plastics. Figure 1-1 is a schematic of Volvo-2009 model [4], showing the different classes of materials used for designing the car body. It can be seen that the bulk of the car body consists of AHSS steels of which DP steel is predominantly used. Hence in the present study an attempt has been made to fabricate low carbon ultrafine grained (UFG) DP steels.

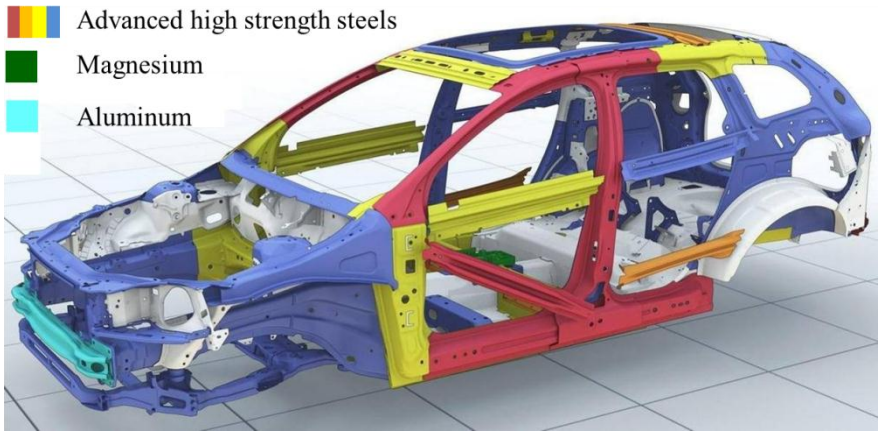

Figure 1-1: A schematic of Volvo-2009 model, showing the different class of materials used for designing the car body [4].

The main challenge in producing DP steels is to achieve grain refinement at the same time making them cost effective. Several processing techniques have been developed to induce grain refinement in steels, for example, Park et al. [5] have used equal channel angular pressing (ECAP), Song et al. [6] have used warm deformation, Azizi-Alizamini et al. [7] have used rapid intercritical annealing. But the potential of these processing routes to be employed industrially is very slim due to the steps involved in these individual processes. ECAP has limitation on sample size and shape; huge deformation at high temperatures is a major drawback of warm-rolling; high heating and cooling rates are the primary drawback of the rapid intercritical annealing method. Moreover, all these processing routes use higher carbon content (>0.15 wt pct) steels which pose problems with weldability.

In this study, an attempt has been made to fabricate lower carbon content DP steels using the method developed by Aziz-Alizamini et al. [7]. A possibility to reduce the heating and cooling rates is also studied. This thesis is organized as follows: Chapter 2 provides a brief review on the early work done on DP steels, DP steel properties, effect of grain refinement and new processing routes for fabricating DP steels. In chapter 3, the objectives of this work are formulated. In

chapter 4, the methodology of the work has been explained. Results are laid out in Chapter 5, followed by discussion in Chapter 6. The conclusions of the present study are laid out in Chapter 7.

2 Literature review

2.1 Introduction: DP steels

DP steel consists of a hard phase, typically martensite (sometimes having a small amount of bainite and/or retained autenite) dispersed in a soft ferrite matrix. Martensite is a supersaturated solid solution of carbon in ferrite with body-centered tetragonal (bct) [8] crystal structure.

DP steels have attractive mechanical properties like low yield ratio, high initial work hardening rate, good uniform elongation for a given ultimate tensile strength (UTS) [9-12] and they also have good crash worthiness. Hence they have gained significant attention, particularly for sheet production of steel for automotive applications.

The chemistry of the DP steels typically contain about 0.05-0.2 wt pct carbon and 1-2 wt pct manganese [13, 14]. In addition, they may contain small amounts of silicon, niobium, molybdenum, and chromium. Carbon is the most important element affecting the hardenability of steel [15] and indeed, the mechanical behaviour of DP steel is to a large extent controlled by the carbon concentration through its effect on the volume fraction and strength of the martensite phase. Manganese is added because it is cost effective in promoting hardenability [15]. Silicon is useful in preventing pearlite and carbide formation and also results in solid solution hardening of the ferrite phase [15-17]. Chromium and molybdenum improve hardenability, suppress pearlite formation and promote martensite formation. Niobium refines the ferrite grain size and results in precipitation strengthening of the ferrite phase [18].

Table 2-1, shows the typical compositions in two different classes of DP steels, i.e. DP 600 (with a minimum UTS of 600 MPa) and DP 800 (with a minimum UTS of 800 MPa). It can be seen that as the ultimate tensile strength (UTS) increases (i.e. from 600 to 800 MPa) higher carbon and alloying contents seem to be required.

Table 2-1: Typical chemical composition of different grades of DP steels (in wt pct)

Grade	C	Mn	Cr	Nb	Si
DP 600	0.1	1.7	0.2	-	0.4
DP 800	0.16	2.0	0.3	0.015	0.4

2.2 Conventional processing techniques of DP steels

Industrially, DP steels are fabricated by two processing routes: either intercritical annealing of cold-rolled steels or hot-rolling followed by fast cooling. In the intercritical annealing process [10, 17, 19] the cold-rolled ferrite-pearlite microstructure is heated to the intercritical temperature range where both ferrite and austenite coexist. The austenite formed is then rapidly cooled to room temperature to transform into martensite. The production route for intercritical

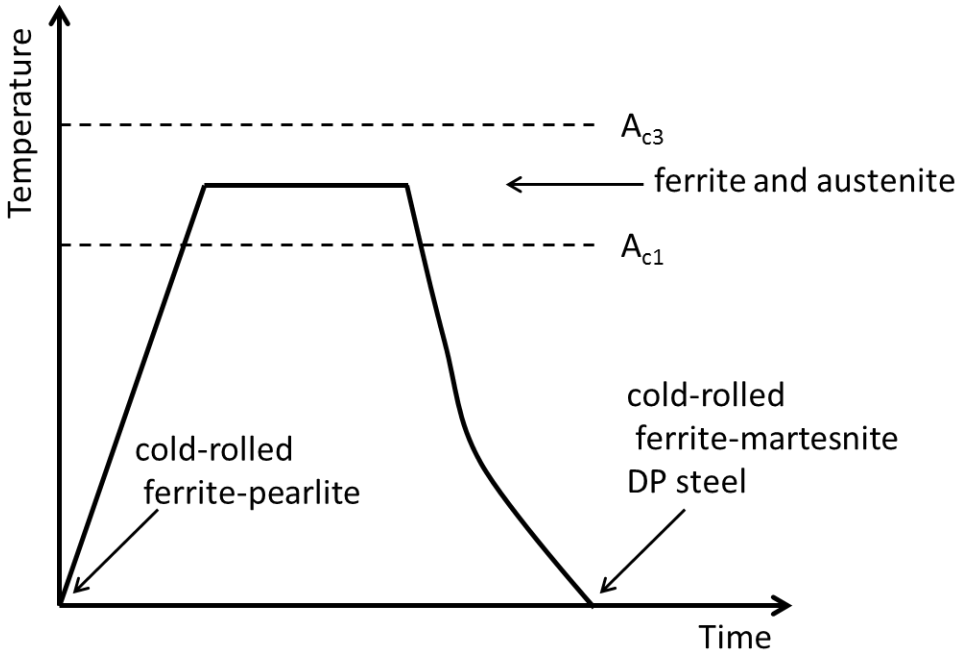

Figure 2-1: Schematic diagram of intercritical annealing process to fabricate cold-rolled DP steel.

annealed DP steels is schematically shown in Figure 2-1, where, A_{c1} and A_{c3} are the start and finish temperatures of austenite formation during heating. The hot-rolling process [10, 20] takes place in the austenitic region. The hot-rolled steel is subsequently cooled into the ferrite-austenite temperature range where desired fraction of ferrite is formed. This is followed by an accelerated cooling step such that the remaining austenite transforms to martensite. The schematic of the production route for hot-rolled DP steels is shown in Figure 2-2, where, M_s and A_{r3} are the martesnite and ferrite start temperatures upon cooling.

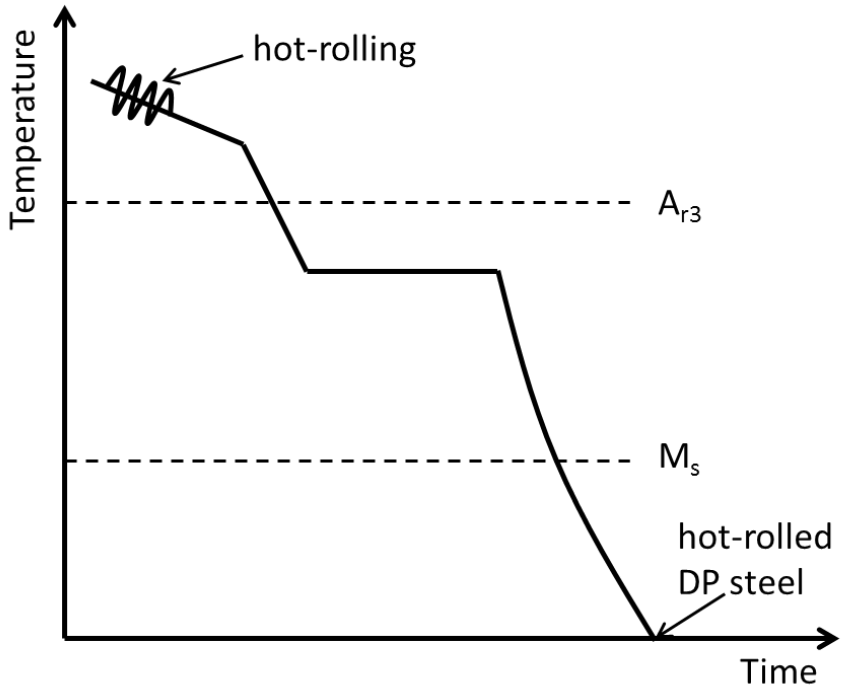

Figure 2-2: Schematic diagram of hot-rolling process to fabricate DP steel.

2.3 Properties of DP steels

2.3.1 Strength

The strength of DP steels primarily depends on the volume fraction of martensite [17, 21, 22] as shown in Figure 2-3. Davies [17] stated that the tensile strength is independent of the strength and composition of martensite. Speich et al. [9] has done work on steels with varying carbon content (ranging between 0 to 0.2 wt pct) and produced similar fractions of martensite with varying carbon levels using different intercritical annealing temperatures. They observed that both the yield and tensile strength increased when the fraction and strength of martensite was increased. They also pointed out that an increase in yield strength is much less pronounced than that of tensile strength with increasing carbon/martensite content.

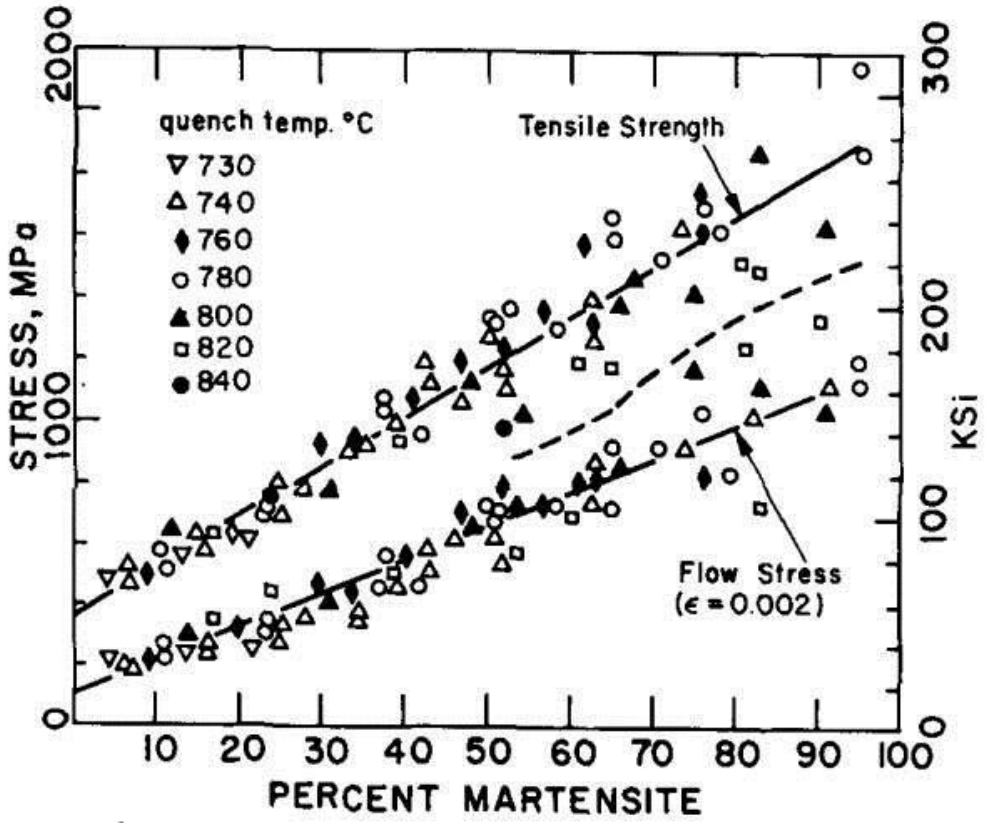

Figure 2-3: The 0.2 pct flow stress and the tensile strength as a function of percent martensite for the Fe-Mn-C alloy [17].

The strengthening effect of martensite has been attributed to three main factors. First, the martensite phase can carry a substantial load which is transferred from the ferrite matrix. Second, martensite can affect the deformation behaviour (flow stress and work hardening behaviour) of the ferrite matrix by introducing internal stress [23, 24]. This is a feature in two-phase materials which results from the strain gradient between the constituent phases with different deformation behaviours. The geometrically necessary dislocations are required to accommodate this strain gradient and to allow compatible deformation of constituent phases. Third, the presence of martensite can affect the ferrite phase due to the additional dislocations introduced into the ferrite structure in the vicinity of martensite islands as a result of the plastic strains associated with the martensite transformation [25-27].

2.3.2 Yield behavior

While undergoing deformation, ferrite phase first starts to plastically deform in a DP steel [28, 29]. Thus, the yielding behaviour of DP steels is controlled by the strength of the ferrite phase [30, 31]. Ferrite yields discontinuously in the absence of martensite, however, it yields differently when used as the matrix in DP steels. The yielding of ferrite in DP steels is continuous suggesting that the initiation of plastic flow in the ferrite matrix occurs in a gradual and continuous manner [28, 32]. The continuous yielding of DP steels can be attributed to the presence of internal stresses within the ferrite matrix originated from the transformation strains associated with the martensite transformation as well as the plastic incompatibility between the constituent phases [28, 33]. Internal stresses cause microyielding of the ferrite at regions around the martensite islands under relatively low applied stresses compared with the yield stress of bulk

ferrite and consequently, plastic flow begins simultaneously in many regions within the ferrite matrix throughout the microstructure.

2.3.3 Work hardening

Dual-phase steels exhibit a characteristic high initial work hardening rate [9, 29, 33, 34]. This rapid increase in work hardening at low plastic strains results from three factors [9]. First, the residual stress generated during quenching [35] is relieved by small amounts of plastic deformation. Secondly, an increase in the dislocation density of the ferrite matrix [36] also helps in work hardening. Thirdly, the plastic incompatibility between two phases leads to the formation of back stresses in ferrite phase. These back stresses restrict dislocation movement in the ferrite phase. Once the residual stresses are eliminated the later stages of plastic deformation are similar to that of ferrite containing other coarse dispersions of hard particles. In a ferrite-cementite system the back stresses are nearly constant at higher plastic strains [37] and presumably, a similar situation exists in ferrite-martensite systems. The effect of the transformation of retained austenite during plastic straining on the work hardening rate [38] is negligible as the amount of retained austenite is minimal in DP steels.

Increase in the martensite content also leads to high initial work hardening rate in DP steels [9, 39]. Martensite island size also affects the work hardening behaviour in DP steels. According to Balliger [12] and Pickering [40], the work hardening rate of DP steels increases with a decrease in the martensite island size. The experimental results regarding the effect of martensite shape on the work hardening behaviour of DP steels are very limited. Sarosiek and Owen [29] have shown that DP steels with banded martensite morphology (mostly continuous) has almost the

same work hardening behaviour as the homogenized DP steel with smaller (noncontinuous) martensite islands.

Mazinani et al. [21] used a low carbon (0.06 wt pct) Fe-C-Mn-Mo steel to compare the effect of martensite morphology on the work hardening behavior of DP steels. Figure 2-4 and Figure 2-5 show the true stress – true strain behavior of DP steels with equiaxed and banded martensite morphology, respectively. Comparison of Figure 2-4 and Figure 2-5 shows that there is a significant difference in the large strain work hardening rates (i.e., measured as the slope of the stress-strain curve from the necking point to fracture) for the samples with different martensite morphologies. For the samples that were heated at 1^{o}C/s to the intercritical temperature (equiaxed martensite islands), the large strain work hardening rate was measured to be approximately 500 to 600 MPa/unit strain and was found to be weakly dependent on the martensite volume fraction, because the slopes are the same as they are parallel to each other. In contrast, for the case of 100^{o}C/s heating rate (elongated martensite islands) to the intercritical temperature, the large strain work hardening rate was found to be in the range of 400 to 675 MPa/unit strain for 18 to 77 pct martensite, increasing with martensite volume fraction, because the slopes increases with martensite content.

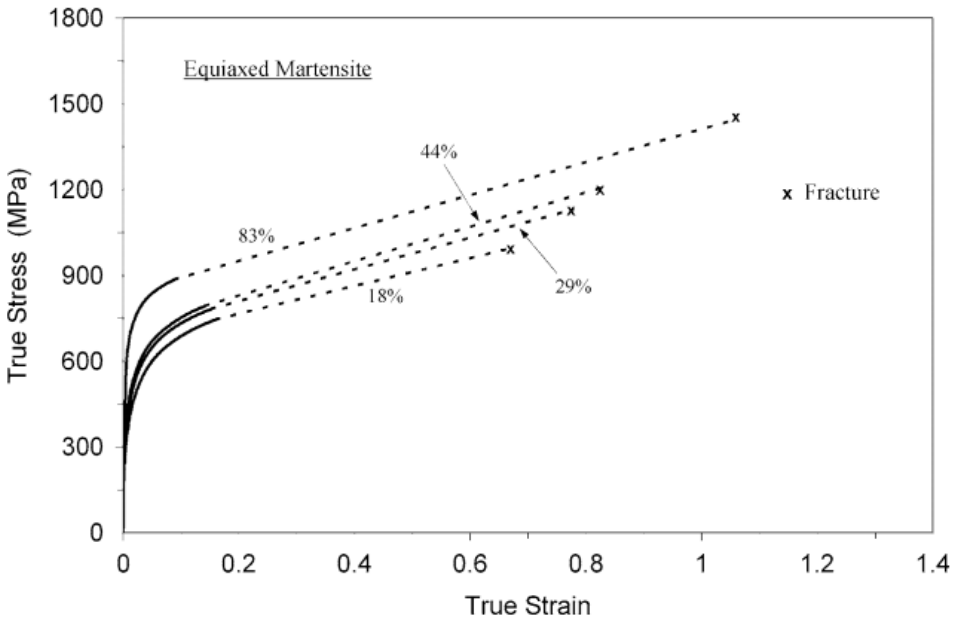

Figure 2-4: True stress–true strain curves of DP steels produced using 1°C/s heating rate to the intercritical annealing temperature for different martensite fractions [21].

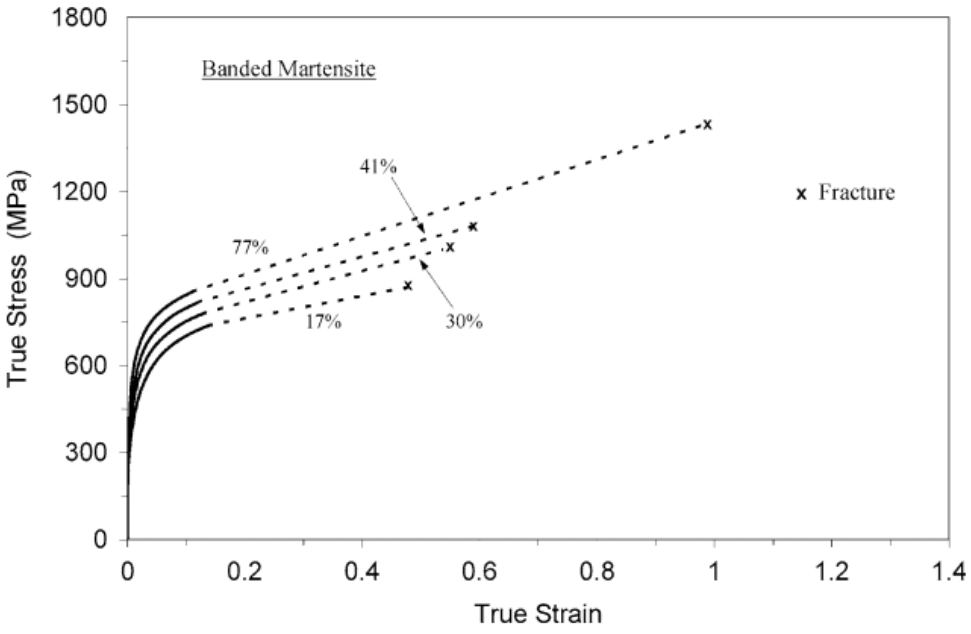

Figure 2-5: True stress–true strain curves of DP steels produced using a 100°C/s heating rate to the intercritical annealing temperature for different martensite fractions [21].

2.3.4 Elongation

For a constant UTS value DP steels have better ductility as compared to commercial HSLA steels [17]. But the uniform elongation, total elongation, and reduction in area all decrease as the amount of martensite and the tensile strength increases. Speich et al. [9] have produced a series of (1.5 wt pct Mn) DP steels by systematically varying the carbon concentration (from 0 to 0.2 wt pct) of the steel and the intercritical annealing temperature (740, 760 and 780^{o}C). The effect of martensite content on the uniform elongation and true strain behavior is shown in Figure 2-6. It is evident form the graph that irrespective of the annealing temperatures an increase in the martensite content has a detrimental effect on the uniform elongation as well as true strain at uniform elongation, and the relationship appears to follow a linear path. The variation of the total elongation with martensite content is shown in Figure 2-7. Here also the martensite content has the same effect, an increase in martensite content deteriorates the total elongation value of the DP steel and the relationship is again linearly dependant. It can also be seen that the same fraction of martensite can be formed for steels with varying carbon content by changing the annealing temperatures. Moreover for a fixed martensite fraction in steel, the elongation increases with increaseing annealing temperature, i.e. higher elongation for martesnite containing lower carbon levels.

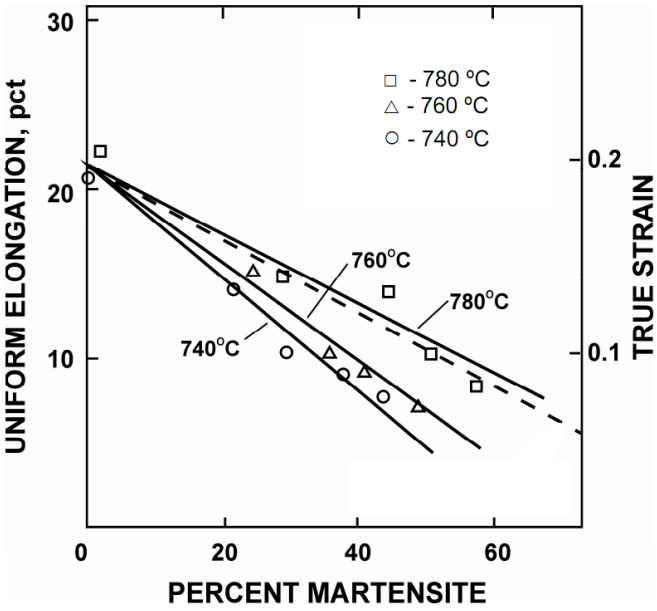

Figure 2-6: Variation of the uniform elongation and true strain of the DP steels with martensite content [9].

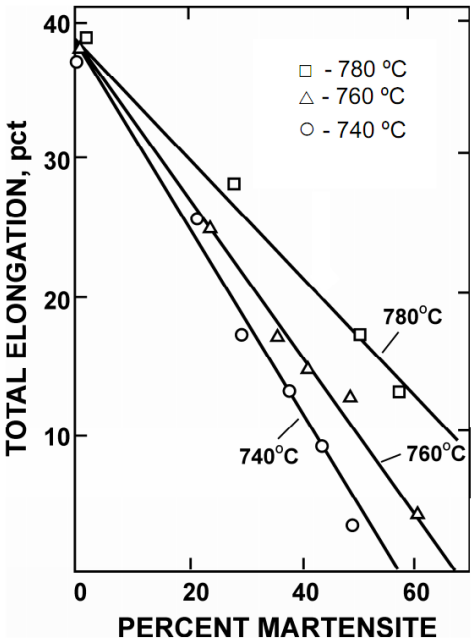

Figure 2-7:Variation of the total elongation of the DP steels with martensite content [9].

2.3.5 Fracture

Balliger and Gladman [12] showed that the replacement of pearlite in the steel microstructure with martensite has a detrimental effect on the total elongation and fracture strain. This is probably due to the fact that the hard and non-deformable martensite phase has an undesirable effect on the damage formation process during deformation. The martensite is usually a brittle phase (depending on its carbon concentration) which may fracture at high strain levels in the non-uniform (post-necking) deformation regime. On the other hand, decohesion at the ferrite-martensite interface due to the plastic incompatibility may also occur in this deformation regime. Both these phenomena are reported as responsible mechanisms for ductile fracture in DP steels [41-47].

But there are reports which suggest that even with the presence of non-deformable martensite, these steels still exhibit ductile fracture behaviour [43, 44, 48, 49]. It has been observed that the ductile fracture in DP steels occurs in three sequential stages, i.e. void nucleation, void growth and void coalescence resulting in a dimpled fracture surface (a characteristic of ductile fracture). Microvoids which are nucleated as a result of the decohesion at the ferrite-martensite interface and/or martensite cracking, usually grow within the more ductile ferrite matrix resulting in a ductile fracture pattern. It should be noted that this effect depends on the martensite content, size and morphology [49-51]. It has been shown in these investigations that large, banded and inter-connected martensite islands in DP steels, compared to the fine and isolated martensite particles, result in poor fracture properties. Mazinani et al. [21] found that irrespective of the martensite fraction, the true strain to fracture is greater by about 0.1 for equiaxed martensite as compared with banded martensite morphology (see Figure 2-8). In summary, the fracture behaviour of dual-phase steels is critically affected by the martensite content, morphology and size [49-53].

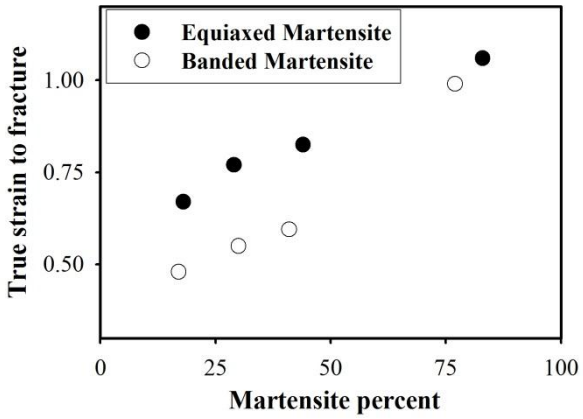

Figure 2-8: Effect of martensite morphology on the true strain to fracture (replotted) [21].

2.4 Strengthening of DP steel

Although DP steels have better mechanical properties as compared to conventional HSLA steels, there is always the desire to improve them further. In particular, the common strengthening mechanisms applied in HSLA steels remain of significance for DP steels, i.e. grain refinement, precipitation hardening, dislocation hardening, and solid solution strengthening [54].

Adding higher Mn content to the steel chemistry is one way to achieve grain refinement. Terao [17] reported that adding high Mn content (3 wt pct) to DP steels resulted in fine dispersion of martensite leading to higher tensile strength and good ductility. Adding alloying elements like Mo, Nb, Ta and B led to further improvement of the mechanical properties of the high Mn DP steels [17,55]. Figure 2-9 shows that Nb microalloying significantly promotes refinement of the DP structure.

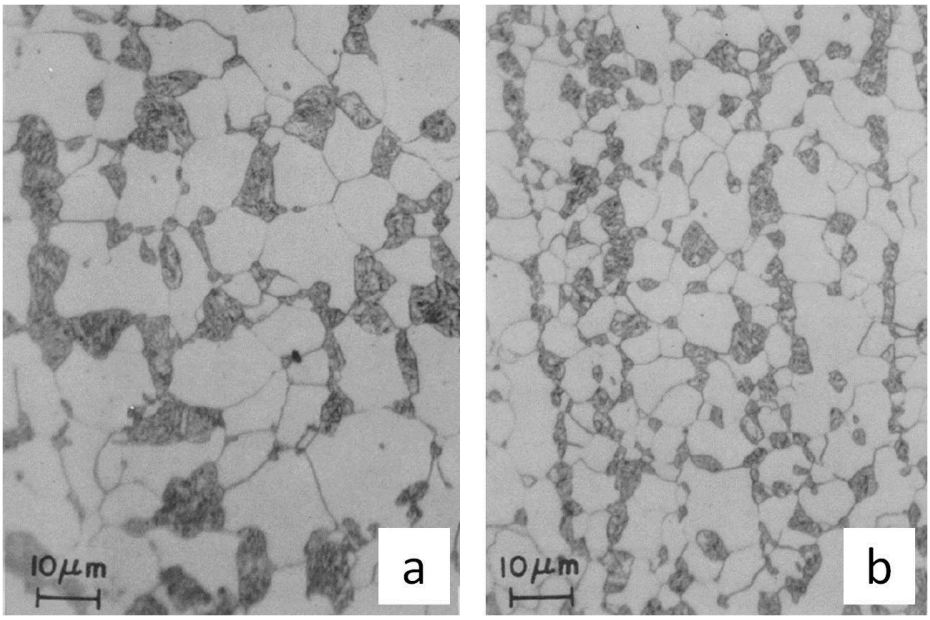

Figure 2-9:Influence of Nb addition on grain refinement in (a) 0.72 Mn, 0.28 Mo (wt pct) steel (b) 0.72 Mn, 0.26 Mo, 0.05 Nb (wt pct) steel [17].

Few studies have been done on the fabrication of fine grain DP steels using alloying additions. Tsipouridis et al. [56] used C-Mn (0.1-1.5 wt pct) steel with 0.8 wt pct Mo and Cr additions to create fine DP structures. Using a constant heating rate of 25^{o}C/s and employing cooling rates below 80^{o}C/s, they achieved yield strengths (YS) between 270-370 MPa and UTS in the range of 660-810 MPa, with about 15% uniform elongation (UE). It is also reported that grain refinement had a positive effect on the YS and UTS values, but no conclusion was made on the hole-expansion behaviour, which plays a crucial role in fracture analysis.

The conventional methods employed to strengthen the DP steels either involved adding additional alloying (increases the material cost) or increasing the carbon content (hinders weldability). So there is scope to design new processing techniques to reduce material cost but with simultaneous improvement of mechanical properties.

2.5 New processing techniques

The conventional approaches (see section 2.2) have been generally followed to commercially fabricate DP steels. But over the years new processing routes have been developed in the laboratory to increase the strength and ductility by microstructure refinement rather than adding alloying elements.

Of the several techniques developed for producing ultrafine grained (UFG) (grain size of the order of 1 μm) materials, the equal channel angular pressing (ECAP) technique introduced by Segal et al. [57] has been successfully applied to produce various bulk UFG materials without residual porosity. A schematic of the ECAP die is shown in Figure 2-10, where Φ is the inner contact angle and Ψ is the arc of curvature at the outer point of contact between channels of the die. During ECAP, the sample was rotated 180^{o} around its longitudinal axis between the passages. This pattern of pressing helps in restoring the shape of the original segment at each even number pass and thereby achieving a nearly equiaxed UFG structure. Shin et al.[58] have used the ECAP technique to obtain fine ferrite grains (0.2-0.3 μm) in a ferrite-pearlite structure. Park et al. [59] combined ECAP with an intercritical annealing step to obtain UFG DP structures in a plain carbon-manganese (Fe-0.15C-1.1Mn (in wt pct)) steel.

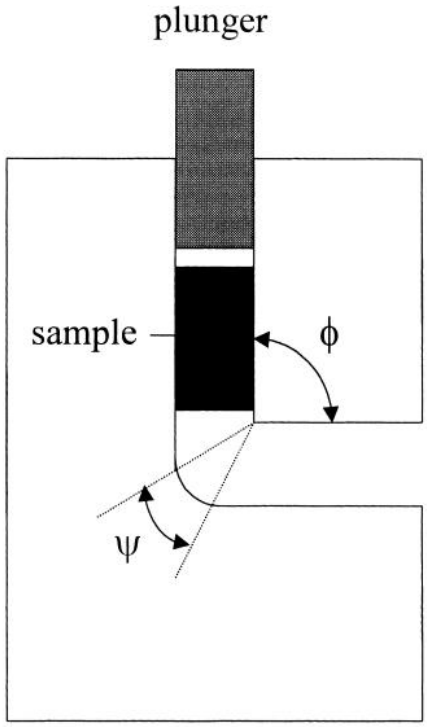

Figure 2-10: A schematic illustration of the ECAP pressing die, where Φ is the inner contact angle and Ψ is the arc of curvature [58].

The ferrite and martensite island sizes were of the order of 1 μm (see Figure 2-11). The yield and tensile strength follow the Hall-Petch relation with respect to the grain size. The UTS and total elongation values for the UFG and coarse grain DP steels are 890, 764 MPa and 17.6%, 13.5% respectively, which clearly shows that the UFG DP steels have superior strength-ductility balance as compared to coarse grain DP steels.

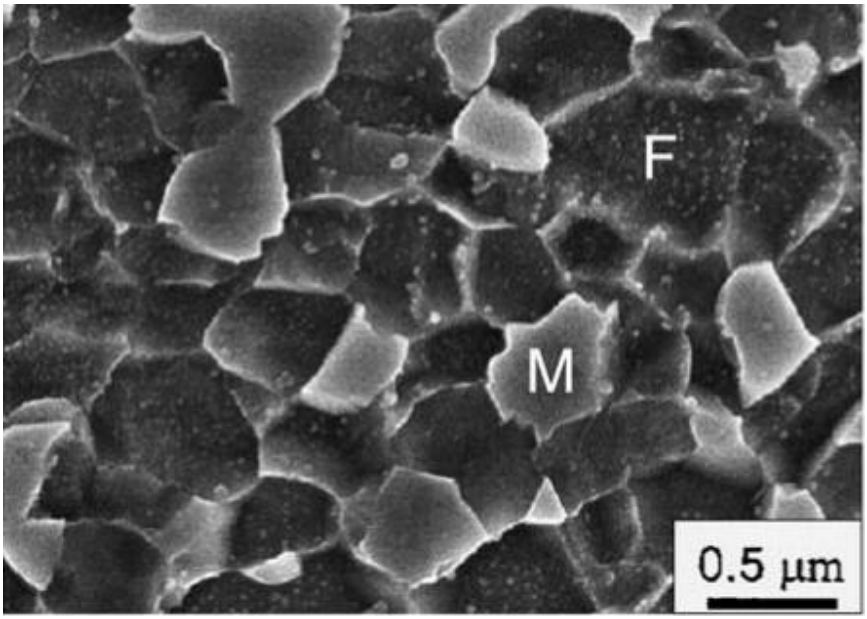

Figure 2-11: DP structure fabricated by ECAP (F-ferrite; M-Martensite) [59].

Mukherjee et al. [60] created fine DP structures using four different low carbon steels (Fe-0.06C-1.8Mn (in wt pct)) with varying amounts of Mo and Nb. They used the deformation-induced ferrite transformation (DIFT) technique to fabricate fine DP structures. Using DIFT they were able to achieve ferrite grain sizes of the order of 1-2 μm. To obtain DIFT, strongly undercooled, metastable austenite is heavily deformed in a temperature range that is usually 25^{o}C to 100^{o}C above the A_{r3} temperature; i.e., the transformation start temperature for the same cooling path but without the deformation step. As phase transformation is a more favorable reaction compared to recrystallization of austenite in this lower temperature regime, deformation at this temperature enhances ferrite nucleation. Significant undercooling below the A_{e3} temperature provides a sufficiently high driving pressure for ferrite nucleation. This enhanced ferrite nucleation results in ultrafine ferrite (UFF) grains. The schematic of the DIFT method is shown in Figure 2-12. The two critical aspects of this process are the absence of an intercritical annealing step and the inclusion of a hot-rolling step. Tensile tests were not performed to measure strength and

ductility, but the predicted values of tensile strength using the hardness data revealed lower strength compared to DP steels processed via ECAP.

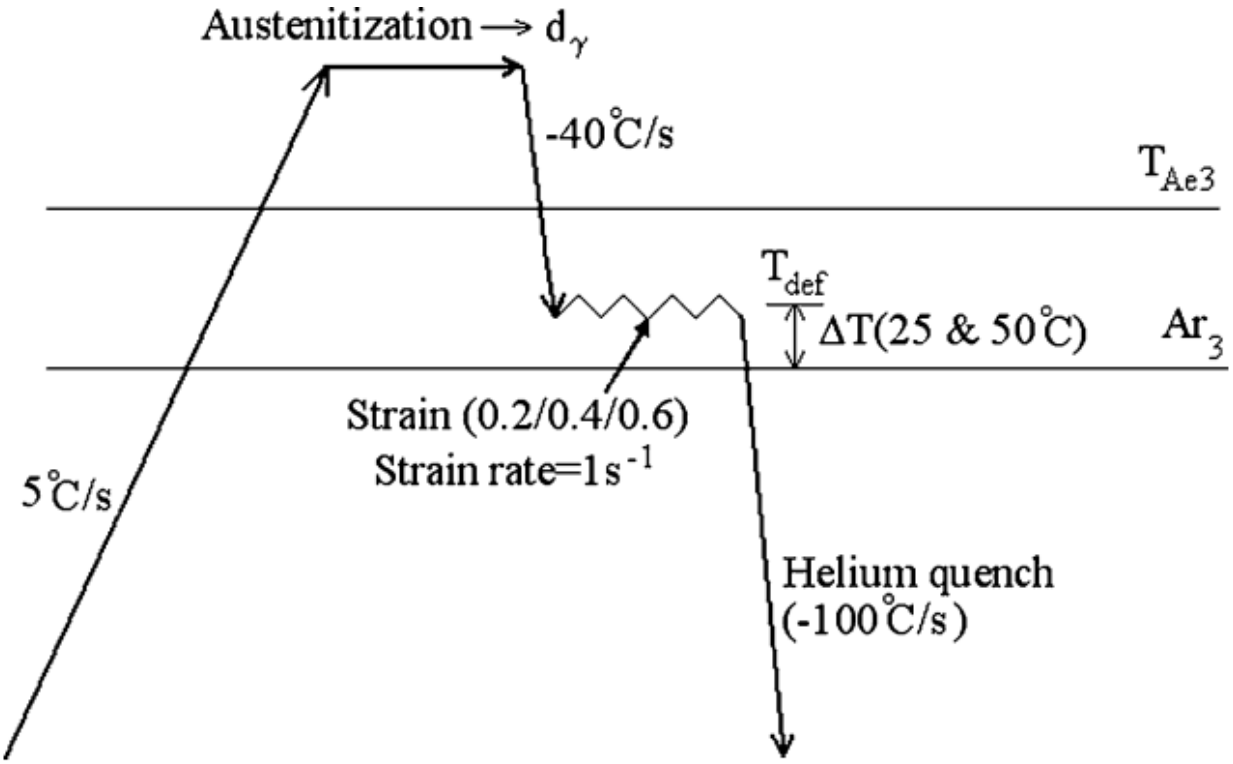

Figure 2-12:DIFT test procedure for fabricating DP steels [60].

Calcagnotto et al. [61] have developed a large strain warm deformation method (see Figure 2-13) to obtain fine ferrite-carbide aggregate in a plain carbon-manganese (Fe-0.17C-1.5Mn (in wt pct)) steel. The first step consists of 3 min of austenitization at 912°C and a single-pass deformation at 860°C applying a logarithmic strain of $\varepsilon = 0.3$ at a strain rate of 10 s^{-1} above the recrystallization temperature. Grain refinement is achieved by subsequent large-strain warm deformation at 550°C. A total strain of 1.6 is realized by a four-step flat compression series, each step exerting a strain of 0.4 at a strain rate of 10 s^{-1}. The large strain warm deformation is used as

a penultimate step prior to intercritical annealing. Intercritical annealing is done at 730°C for 3 min and subsequent quenching to obtain the final ferrite/martensite DP microstructure (see Figure 2-14). They have obtained an average grain size of 1.2 μm.

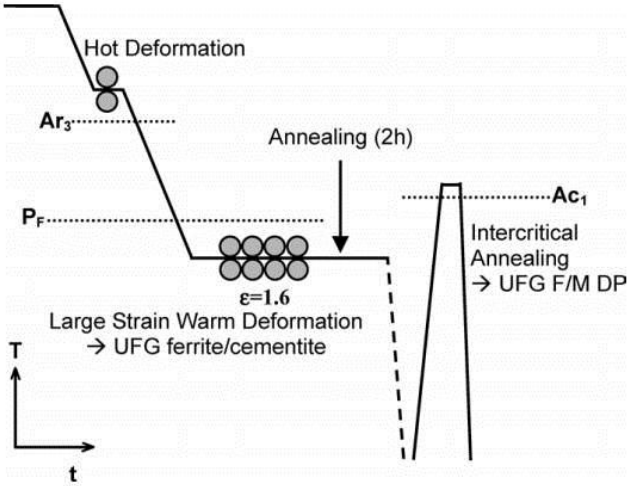

Figure 2-13: Warm-rolling process designed to obtain UFG DP steels, where Ar_3: non-equilibrium transformation start temperature; Ac_1: Austenite start temperature on heating; P_f: pearlite transformation finish temperature; ε: logarithmic strain; T: Temperature; t: time [61].

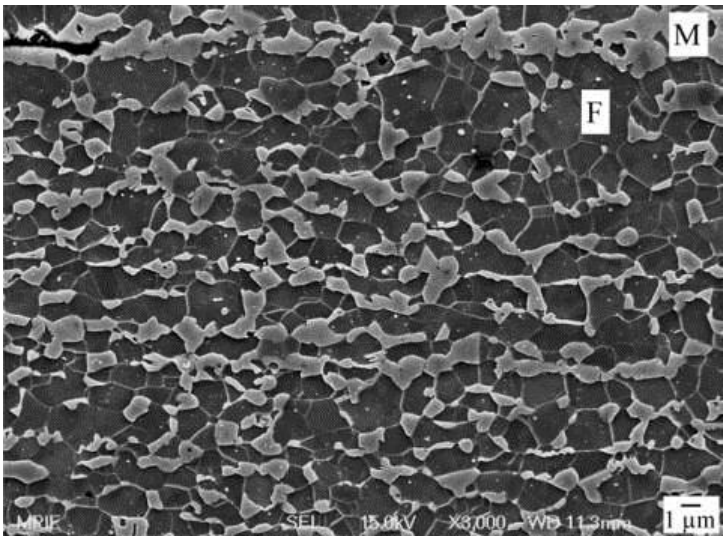

Figure 2-14:UFG DP steel fabricated using large strain warm deformation for a 0.17 C-Mn steel [61].

The UTS and yield strength of UFG and fine grain (FG) DP steels are larger as compared to the coarse grain (CG) DP steels (see Figure 2-15), similar to the one obtained by Park et. al. [59]. The UTS values for the coarse and UFG DP structures are 870 and 1037 MPa respectively.There is no effect of grain size on uniform elongation. The initial strain hardening rate and the post-uniform elongation increase as the grain size decreases. The energy absorption curves for different grain sizes are shown in Figure 2-16. Impact toughness is improved by grain refinement which is revealed by a lower ductile-to-brittle transition temperature and an increase in both upper and lower shelf energy.

Grain refinement promotes ductile fracture mechanisms in response to both tensile and impact conditions. The formation of martensite cracks and cleavage fracture in ferrite is suppressed in the fine grained and the UFG DP steels due to the small size, the more homogeneous distribution and more spherical shape of martensite islands.

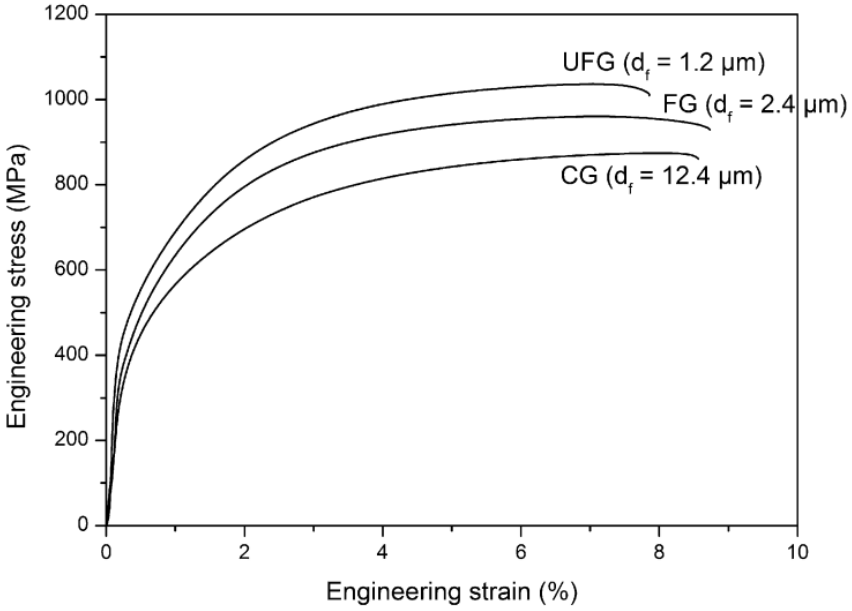

Figure 2-15: Stress strain curves of UFG, fine grain (FG) and coarse grain (CG) DP steels, where d_f is the grain size [62].

Calcagnotto et al. [62] have also studied the role of Mn content in UFG DP steels and reported that a critical amount of Mn content is necessary to avoid grain growth during intercritical annealing and to ensure sufficient hardenability such that the remaining austenite transforms into martensite upon cooling. The grain size is stabilised by (1) lowering the Ac_1 temperature and thus, the intercritical annealing temperature, (2) broadening the ferrite+austenite+cementite three-phase field in which grain growth is inhibited, (3) refining cementite, which causes a more efficient pinning effect and, (4) reducing the grain boundary mobility by solute drag.

The hardenability is primarily dependant on the carbon content but it is also controlled by Mn partitioning between ferrite and cementite, which is established during large strain warm deformation.

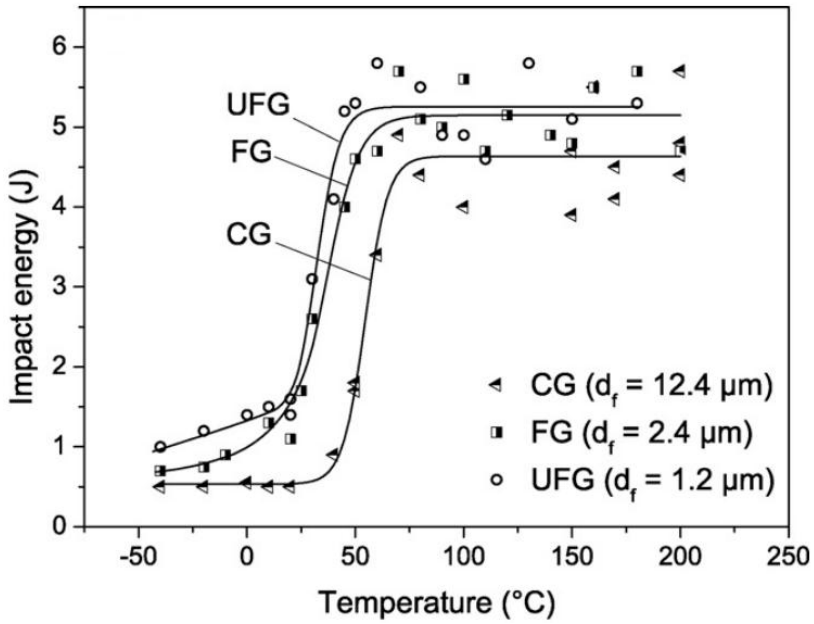

Figure 2-16: Comparison of energy absorption curves for DP steels with different grain sizes [62].

Azizi-Alizamini et al. [7] has developed a novel technique which has the potential to be employed in industry for sheet production of steel. The processing route is shown in Figure 2-17. Initially the cold-rolled ferrite-pearlite structure in an Fe-0.17C-0.74Mn (in wt pct) steel is

austenitised at 1000^{o}C for 30 minutes and subsequently quenched to room temperature using ice-brine to obtain martensite. The martensite is tempered at 550^{o}C for 1 hr to lower the hardness for subsequent 80% cold reduction. Fine ferrite-carbide aggregates are formed (see Figure 2-18) after the final annealing step at 550^{o}C for 75 min. This microstructure is then heated at 300^{o}C/s to the intercritical region (750^{o}C held for 10seconds) and subsequently quenched to room temperature to get UFG DP steels (see Figure 2-18). The average grain size of the DP structure is of the order 1-2 μm.

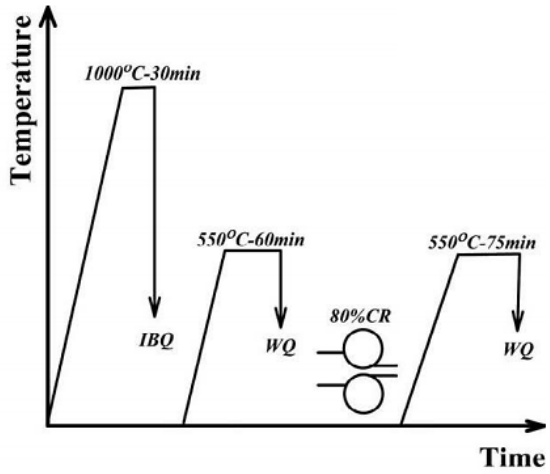

Figure 2-17: Processing route developed to produce fine ferrite-carbide aggregate, where IBQ: ice brine quench; WQ: water quench; CR: cold rolling [7].

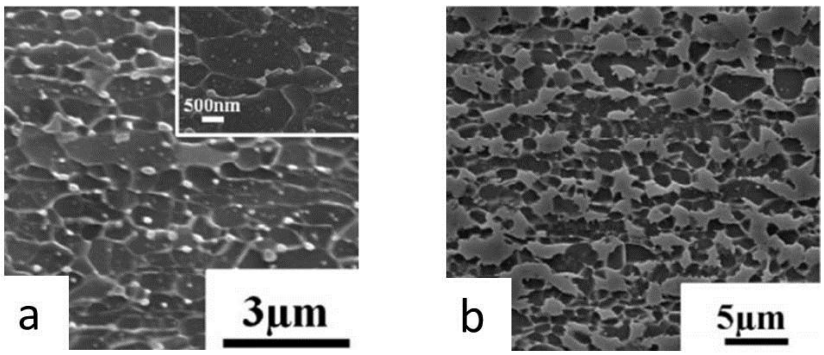

Figure 2-18: (a) Fine ferrite carbide aggregate (b) UFG DP structure for 0.17 C-Mn steel [7].

Figure 2-19 shows the UTS v/s uniform elongation for various DP structures that have been fabricated over the last 4 decades. UFG DP steels fabricated by rapid intercritical annealing have superior properties as compared to conventional DP steels and they are comparable to the DP steels fabricated by ECAP approach (see Figure 2-19). The UFG DP steels have higher UTS values by at least 100MPa as compared to the conventional DP steels, which primarily have a coarse microstructure. The drawback of the rapid intercritical annealing approach is high heating/cooling rates. Nevertheless, further studies could be useful to quantify in more detail whether rapid intercritical annealing is amenable for industrial production of steels.

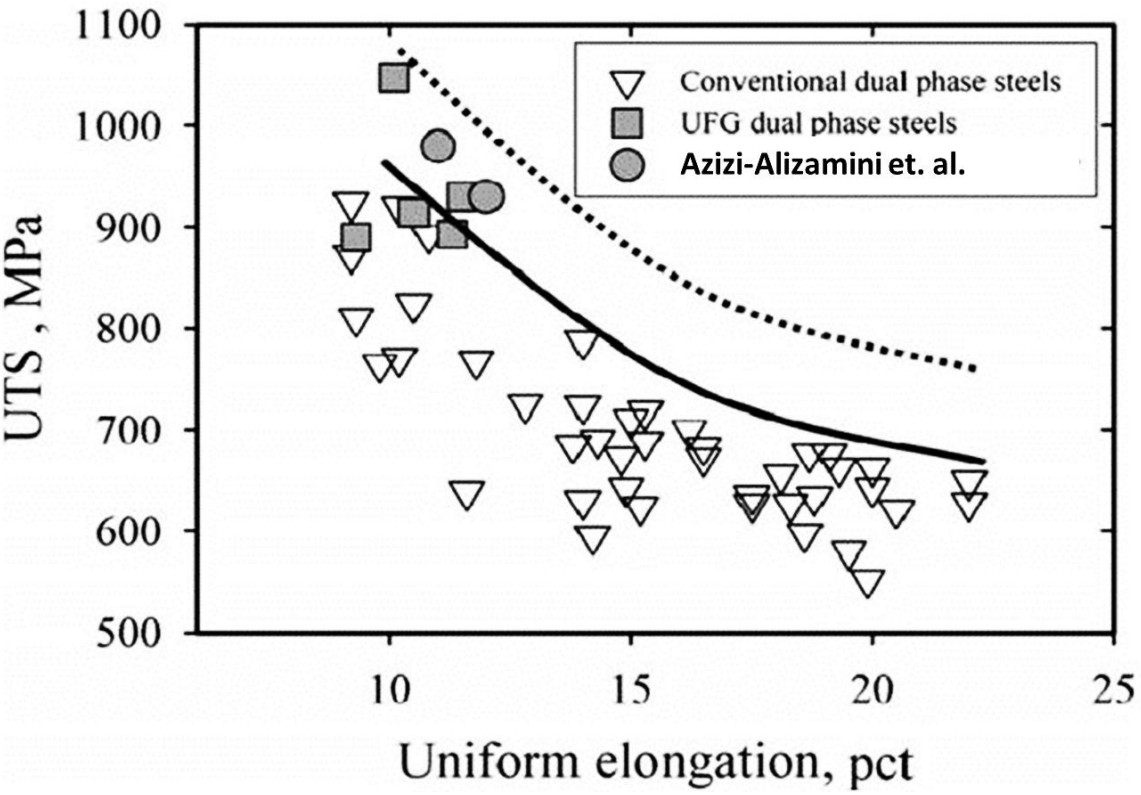

Figure 2-19:UTS v/s Uniform Elongation for various DP steels [7].

.

3 Objectives

The goal of this work is to evaluate the feasibility to apply rapid intercritical annealing method developed by Azizi-Alizamini et al. [7] to lower carbon (≤ 0.1 wt pct) steels (better weldabiligy) and to quantify the effect of lower heating and cooling rates on the DP microstructure and mechanical properties.

To accomplish this overall goal, the following sub-objectives are designed:

- To quantify the austenite formation using dilatometry.
- To quantify the effect of carbon content on the microstructural evolution and mechanical properties of the DP steels.
- To quantify the effect of processing parameters (heating, cooling rate; holding time and temperature) on the DP steel mechanical properties.
- To quantify the effect of different starting microstructures on the final DP steel properties.

4 Methodology

4.1 Materials

Two classes of steels are used in this study. The first category consists of two laboratory plain carbon steels with similar manganese content and different carbon levels, [0.06 and 0.12 wt. pct C, 0.06C and 0.12C steels, respectively] shown in Table 4-1. The 0.06C steel was received as hot-rolled plate from CANMET and the 0.12C steel was as-forged bars from ArcelorMittal Dofasco. The second class of steels are Mo and Nb containing low carbon steels. The Mo-bearing steel (DP 600) was received as a cold-rolled (55%) commercial sheet supplied by Stelco Inc. (now US Steel Canada), Hamilton, ON. The Nb-containing steel was provided as laboratory hot-rolled plate by CANMET. These two steels had similar manganese and carbon content as shown in Table 4-2.

Table 4-1: Chemical composition of plain carbon steels in wt pct

Steel	Fe	C	Mn	Si	Al	N
0.06C	Bal.	0.06	1.8	0.08	0.041	0.006
0.12C	Bal.	0.12	1.5	0.2	0.045	0.006

Table 4-2: Chemical composition of Mo and Nb containing steels in wt pct

Steel	Fe	C	Mn	Si	Al	Nb	Mo
Mo Steel	Bal.	0.06	2.0	0.07	0.037	-	0.15
Nb Steel	Bal.	0.06	1.78	0.092	0.036	0.06	-

The as-received samples were cold-rolled to 4mm thickness using a laboratory mill (roll diameter: 130 mm) and then subjected to thermo-mechanical treatments explained in the following section.

4.2 Thermo-mechanical treatments

4.2.1 Introduction

The aim of the thermomechanical treatment was to develop UFG DP steels. To achieve this goal, the effect of processing parameters and carbon/alloying content on the final microstructures was systematically investigated. To develop UFG DP steels in plain carbon steels, two different types of initial structures, i.e. martensite and fine grained ferrite-carbide aggregates were developed. For Mo and Nb containing steels, however, only the potential to form the fine grained ferrite-carbide structure was examined. The individual processing steps are described below.

4.2.2 Developing initial structures in plain carbon steels

The experimental procedure developed by Azizi-Alizamini et al. [7], was followed to create fine ferrite-carbide aggregates. The processing steps are shown in Figure 4-1. Initially ferrite-pearlite structures were austenitized at 950^{o}C for 10min followed by water quenching (stage 1). This stage is aimed at developing a martensite structure. Then an annealing stage was performed at 550^{o}C for 1h. The resulting tempered martensite was subsequently 80 pct cold-rolled (multiple passes) in a laboratory mill (roll diameter: 130 mm). Cold-rolled sheets were then annealed at 550^{o}C for 1-3 hours depending on carbon content. The 0.06C steel alloy was annealed for 1h and the 0.12C steel was annealed for 3hrs. These processing procedures resulted in fine grained ferrite-carbide aggregates for both steels.

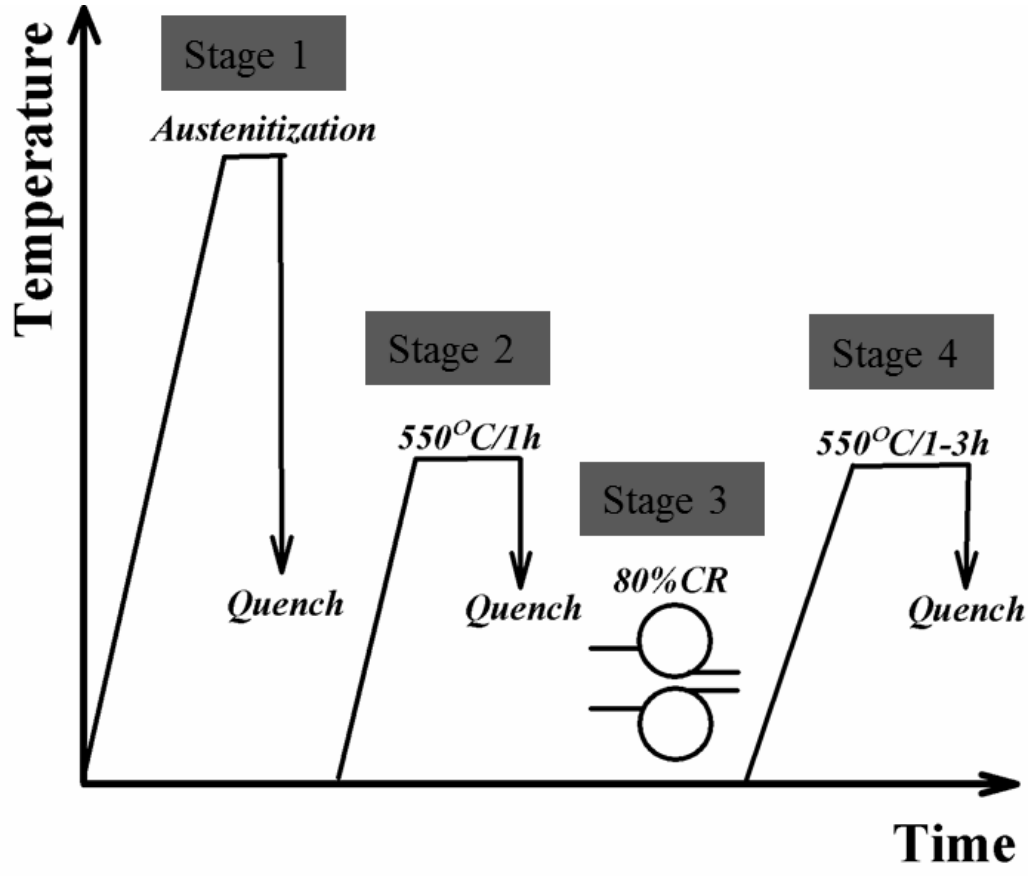

Figure 4-1: Thermo-mechanical treatment performed on plain carbon steels to develop fine grained ferrite-carbide aggregates.

For the sake of comparison, the martensite microstructure developed in stage 1 in Figure 4-1 has also been used as an initial structure prior to intercritical annealing to produce DP steels. All annealing treatments were conducted in a tube furnace with Ar controlled atmosphere.

4.2.3 Developing initial structures in Mo and Nb containing steels

First, the processing route adopted for plain carbon steels, shown in Figure 4-1, was employed for both these steels. As an alternative, a warm rolling process, shown in Figure 4-2, was used to replace the cold rolling and annealing process route for the Mo containing steel. Here, after the first tempering stage, samples were held for 10min at two different temperatures, i.e. 650 and

700^{o}C, respectively, immediately followed by 80 pct reduction (in 4-5 passes) and subsequently air cooling to room temperature.

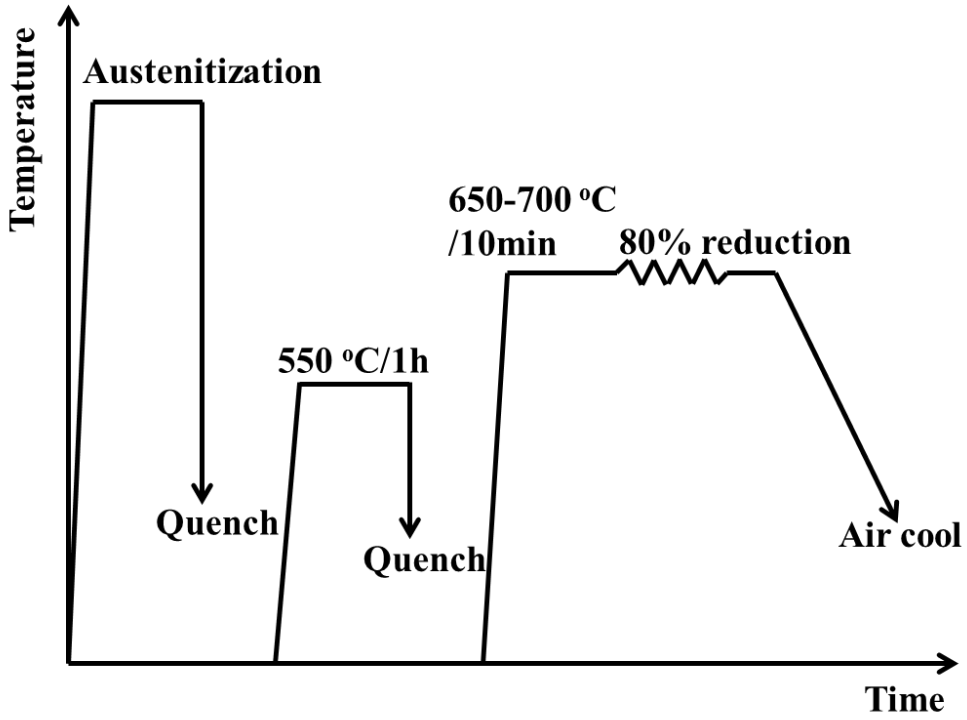

Figure 4-2:Thermo-mechanical process employed for Mo containing steel.

4.2.4 Austenite formation experiments

Initial structures developed as described above were then heated into the intercritical annealing region where ferrite and austenite coexist. Austenite formation is a critical phenomenon during intercritical annealing. Thus, before performing intercritical annealing experiments, a set of austenite formation studies was conducted to investigate the effect of heating rate and initial structure on the austenite formation kinetics.

A Gleeble 3500 thermo-mechanical simulator was employed for all the austenite formation experiments. Test coupons of 60×10×0.8 mm (length×width×thickness) from the fine ferrite-

carbide and 60×10×2 mm from the martensite starting microstructures were cut with the longitudinal direction aligned along the rolling direction. Dilatometry experiments were performed to quantify the transformation kinetics, see Figure 4-3. Larger size samples, 93×12×0.8mm for ferrite-carbide and 93×12×2mm for martensite starting microstructures, were also processed to produce tensile test samples.

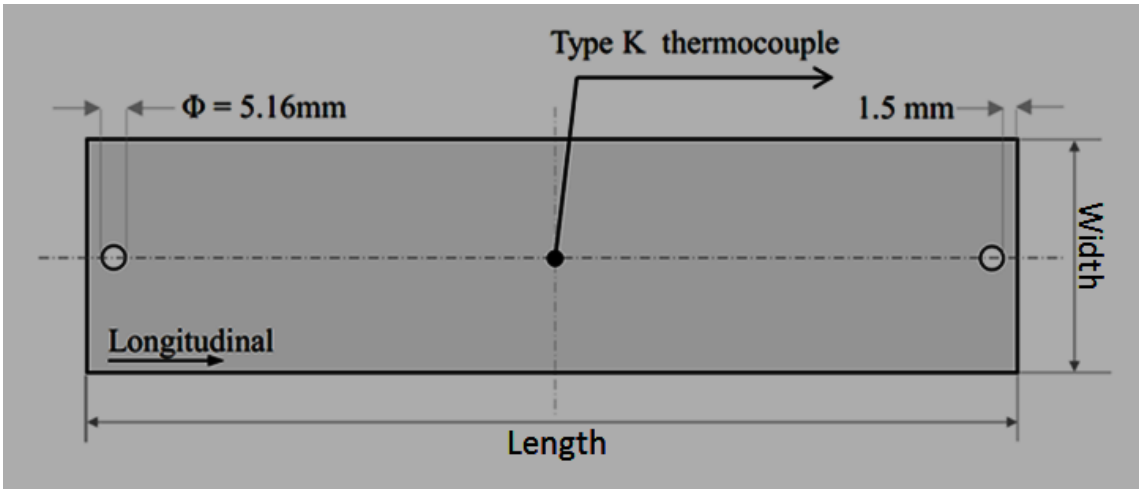

Figure 4-3: Schematic illustration for the dimension of the Gleeble test sample.

The temperature was controlled using a type K thermocouple spot-welded on the centre of the sample. Dilatometry tests were conducted under high vacuum (≈ 0.26 Pa (2.0×10^{-3} Torr)). Continuous heating tests were performed with heating rates 1°C/s, 10°C/s and 100°C/s to systematically investigate the effect of heating rate on microstructure evolution and mechanical properties. A dilatometer was attached to the centre of the samples to measure the change in width during heating. The austenite formation, start (Ac_1) and finish (Ac_3) temperatures upon heating are shown in Figure 4-4. The volume fraction of austenite was determined by analyzing the dilatometric data using the lever-rule. The volume fraction of the austenite formed at a particular temperature can be found using Equation 4-1 as shown below.

$$\text{Volume fraction of austenite} = \frac{AO}{AB} \qquad \text{Equation 4-1}$$

To analyze the microstructure during heating, additional samples were then subjected to interrupted heating tests via quenching between Ac_1 and finish Ac_3 temperatures.

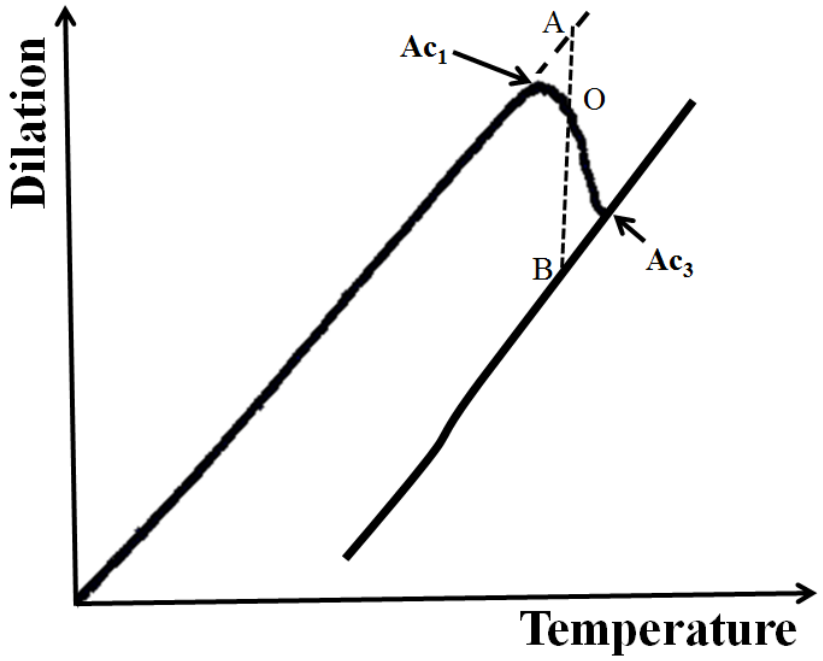

Figure 4-4: Dilatometry test experiment upon continuous heating. Ac_1 and Ac_3 are austenite formation start and finish temperatures during heating.

4.2.5 Intercritical annealing stage

With the knowledge gathered using the austenite formation experiments, the intercritical annealing stage was designed to achieve an austenite fraction of approximately 0.2 (martensite upon quenching). The holding time at intercritical annealing temperature was fixed at 30s and three different heating rates, 1°C/s, 10°C/s and 100°C/s were used. To ensure similar martensite fractions, different intercritical annealing temperatures were adopted for different steel chemistries. Two different quenching media, water and helium, were examined to investigate the effect of cooling rates on the final microstructure and mechanical properties. The intercritical annealing is schematically presented in Figure 4-5.

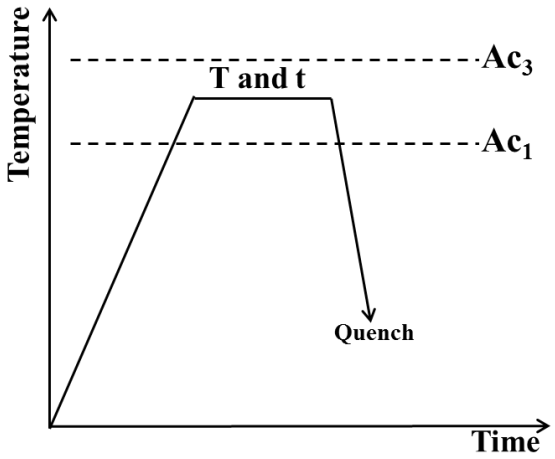

Figure 4-5: Schematic of intercritical annealing, where T and t represent temperature and time of intercritical annealing respectively.

To determine the volume fraction of martensite formed during holding, samples were continuously heated to the intercritical temperatures and held there for 30seconds, followed by continuous heating in to the austenite single phase region and subsequently air-cooled to room temperatures. The schematic is shown in Figure 4-6.

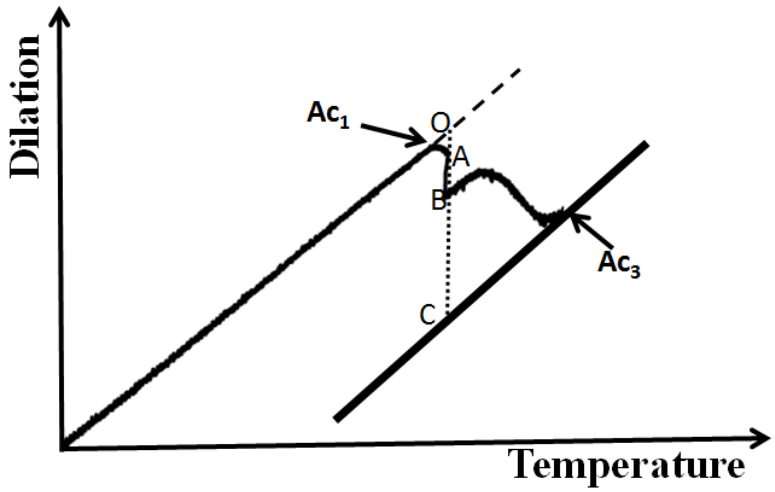

Figure 4-6: Dilatation experiment during holding at the intercritical annealing stage. Ac_1 and Ac_3 are austenite formation start and finish temperatures during heating.

The volume fraction of austenite at 1 and 30 seconds holding is given by Equation 4-2 and Equation 4-3, respectively.

$$\text{Volume fraction of austenite (1 seconds holding)} = \frac{OA}{OC} \qquad \text{Equation 4-2}$$

$$\text{Volume fraction of austenite (30 seconds holding)} = \frac{OB}{OC} \qquad \text{Equation 4-3}$$

4.2.6 Microstructure characterization

Microstructural analysis was carried out along the transverse direction (TD), i.e. the plane perpendicular to both the rolling and normal directions. Microstructures were characterized using Hitachi S2300 and S3200 scanning electron microscopes with a secondary electron detector.

Prior to scanning electron microscopy (SEM), the specimens were polished with SiC polishing papers with grit sizes starting from 60 followed by 400, 600 and ending with 1200. Then the specimens were polished with 6 µm followed by 1 µm diamond solution. The final stage of polishing was an electropolishing step using 95 pct acetic acid and 5 pct perchloric acid solution. Then, the samples were etched with 2 pct Nital solution for 10-15 seconds.

Grain size as well as carbide particle size measurements were based on the equivalent area diameter (EQAD) approach, where the area of the grain is calculated first and assuming the grain as a circle the diameter of the grain is found. At least 1000 grains were analyzed, to have a statistical significance of grain size and grain size distribution. The quantitative measurements were conducted using Clemex image analysis software. Volume fraction measurements were carried out by painting the martensite islands from SEM micrographs and then using the image analyzing software the area of the painted grains are calculated. At least 10 frames/micrographs

are quantified to reduce the scatter in the data. For equiaxed grains, area fraction of the martensite grains is assumed analogous to the volume fraction.

4.2.7 Mechanical properties

To quantify mechanical properties, first hardness measurements were carried out on transformation samples using a Micromet-3 micro hardness tester with 1 kg load. Further, tensile tests were conducted on samples with 12.5mm gauge length as depicted in Figure 4-7 at a nominal strain rate of 2×10^{-3} s^{-1} using a MTS servo-hydraulic machine. An extensometer was used to measure the axial elongation of the tensile sample. The reported tensile test results are the average of at least two tests.

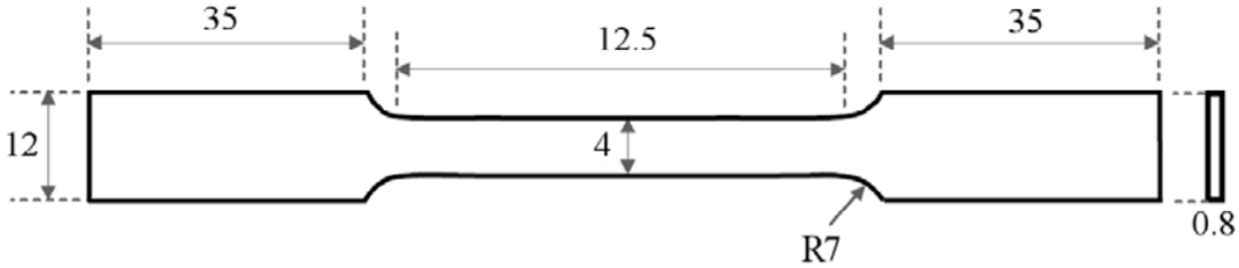

Figure 4-7: Subsize tensile specimen according to the ASTM E8, dimensions are in 'mm'.

The initial cross section area (A_i) of the tensile sample with in the gauge length was measured using screw gauge with a least count of 0.01mm prior to the tensile test. The final fracture area (A_f) was measured using SEM. Then, strain to fracture (ε_f), as a measure of ductility, was calculated using Equation 4-4.

$$\varepsilon_f = \ln\left(\frac{Af}{Ai}\right) \qquad \text{Equation 4-4}$$

UTS is calculated by dividing the maximum load attained during the course of the tensile test by the initial cross-sectional area, and UE is calculated by using the extension in the extensometer at UTS. UTS multiplied by UE gives the strength-elongation balance value, which is an important factor to evaluate the formability of high strength sheet materials. The total elongation (TE) is calculated by using the reading of the extensometer just prior to fracture. 0.2 pct offset method is used to calculate the yield strength (YS) and the yield ratio is found by dividing YS by UTS.

5 Results

5.1 Plain carbon steels

5.1.1 Formation of fine ferrite-carbide aggregates

Ferrite-pearlite is the starting microstructure for both the 0.06C and the 0.12C steels, as shown in Figure 5-1. Ferrite is the dark grey area and pearlite appears as lighter area with a characteristic lamellar structure in the micrograph. This starting material has been cold rolled to 4mm thickness and subsequently austenitized at 950^{o}C for 10 minutes, followed by quenching to room temperature to obtain martensite as shown in Figure 5-2. The martensite phase for both steels has predominantly a lath structure.

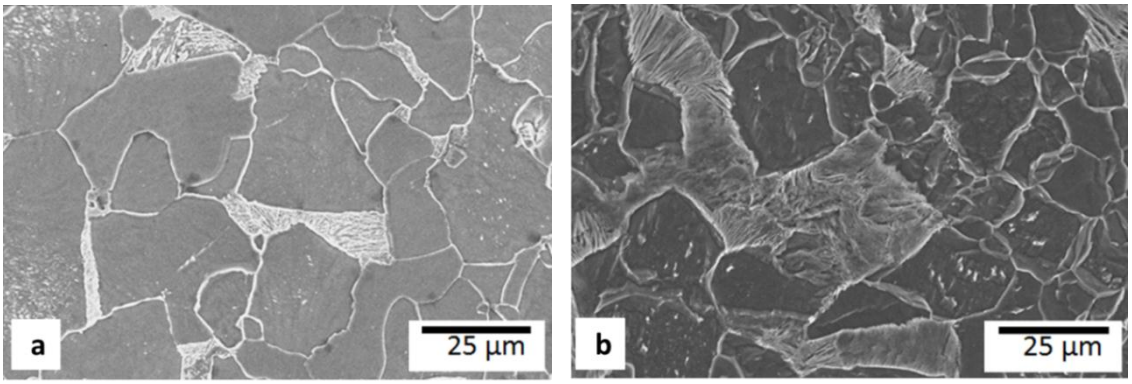

Figure 5-1: Initial ferrite-pearlite microstructures of (a) the 0.06C and (b) the 0.12C steels.

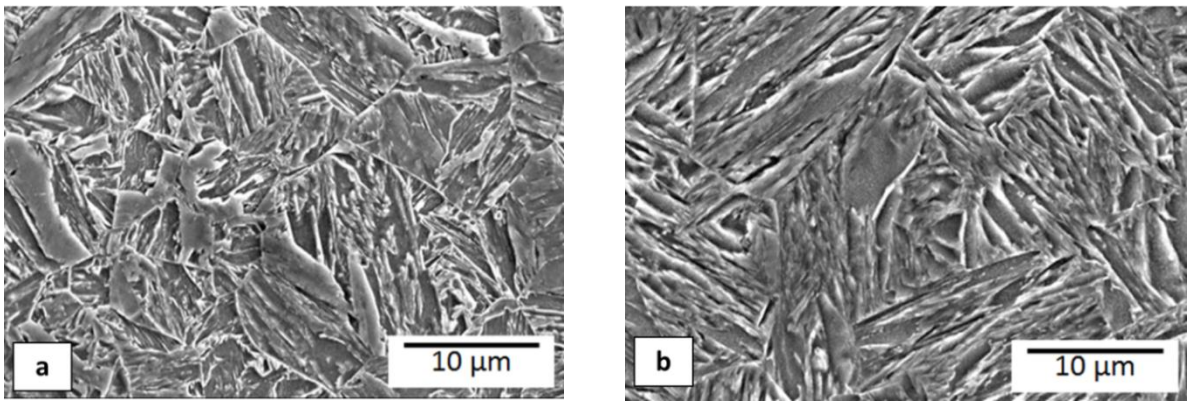

Figure 5-2: Martensite structures of (a) the 0.06C and (b) the 0.12C steels.

Since martensite is a hard phase, a tempering step (550^{o}C for 1 h) has been introduced prior to cold-rolling to soften the martensite and obtain a tempered martensite structure, shown in Figure 5-3. This process makes it easier to perform cold reduction. The Vickers hardness for the initial martensite structures is 342HV and 361HV for the 0.06C and 0.12C steel, respectively, whereas for the tempered martensite the hardness dropped to 225HV and 243HV, respectively, i.e. a significant drop of over 100HV. The carbide particles in the tempered martensite are generally found along the lath and prior austenite grain boundaries. These lath martensite structures were subjected to 80 pct cold recuction. The cold-rolled tempered martensite structure is shown in Figure 5-4.

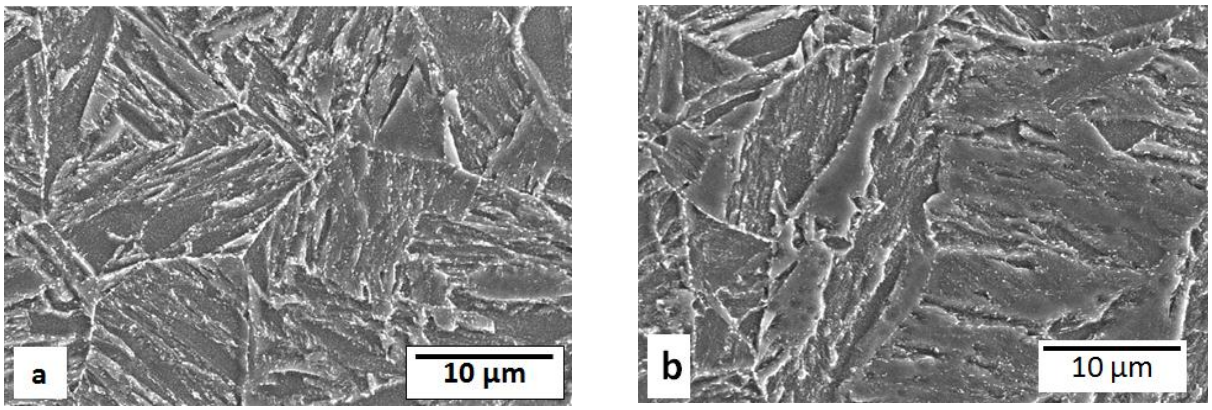

Figure 5-3: Tempered martensite structure of (a) the 0.06C and (b) the 0.12C steels.

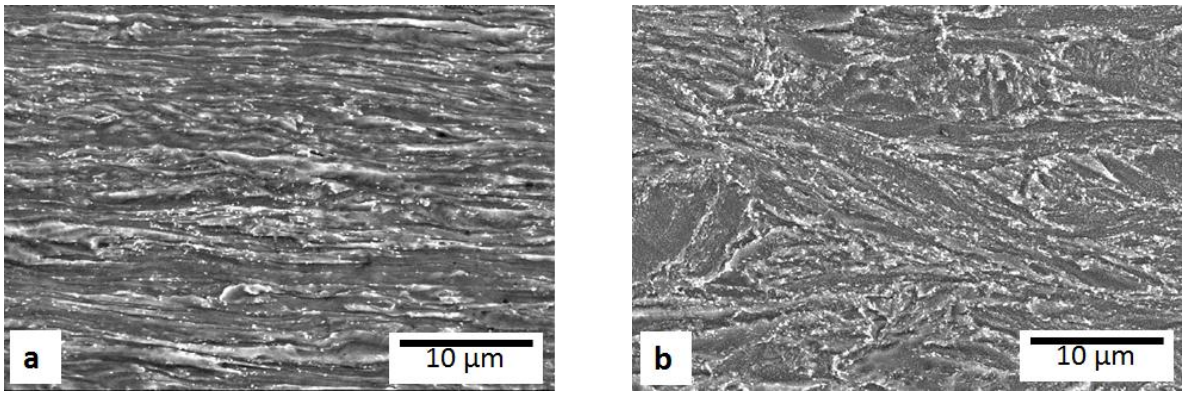

Figure 5-4: 80 % cold rolled tempered martensite structure of (a) the 0.06C and (b) the 0.12C steels.

After an additional tempering step at 550^{o}C fine ferrite-carbide aggregates are obtained, as shown in Figure 5-5. The tempering time is 1h for the 0.06C steel but a fine ferrite-carbide structure was only obtained by increasing the tempering time to 3 h in the 0.12C steel.

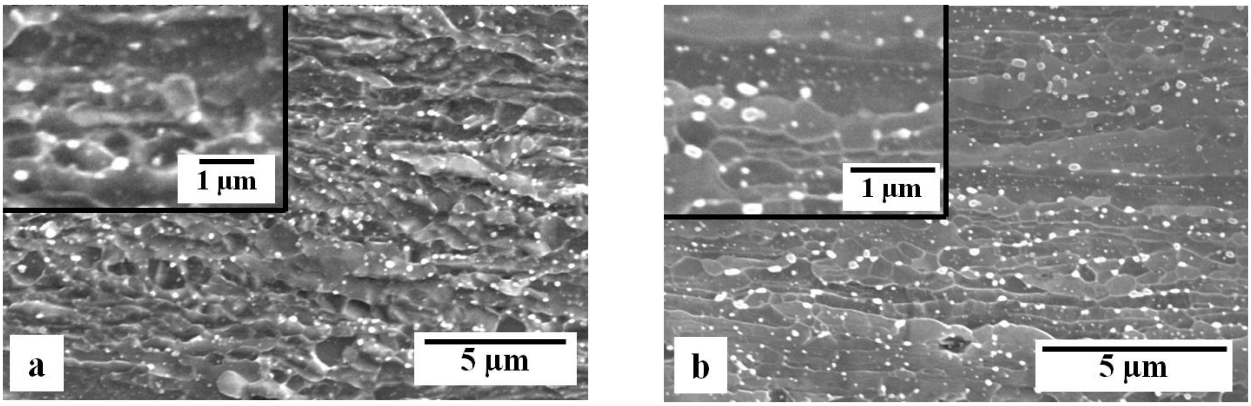

Figure 5-5: Fine ferrite-carbide aggregates of (a) the 0.06C and (b) the 0.12C steels. Higher magnification images are shown as insets.

The ferrite matrix seems to be a recrystallized structure. The carbide particles are distributed in the ferrite matrix. There is a range of carbide sizes. The larger carbide particles form at the ferrite grain boundaries, particularly at the triple junction sites. Finer carbide particles are generally found within the ferrite matrix. The average size of the carbide particles is around 150 nm. The carbide particle distribution is shown in Figure 5-6. The carbide particle size ranges between 100 and 300 nm. For every unit area (1µm^2), two carbide particles are found at the ferrite grain boundaries and one carbide particle inside the ferrite matrix for the 0.06C steel. For the 0.12C steel, three and two carbide particles are present per µm^2 at the ferrite grain boundary and inside the ferrite grains, respectively. The equilibrium mole fraction of carbide particles for the 0.06C and 0.12C steel are 1.11×10^{-2} and 2.05×10^{-2}, respectively i.e. almost twice the amount of carbide fraction for the 0.12C as compared to the 0.06C steel.

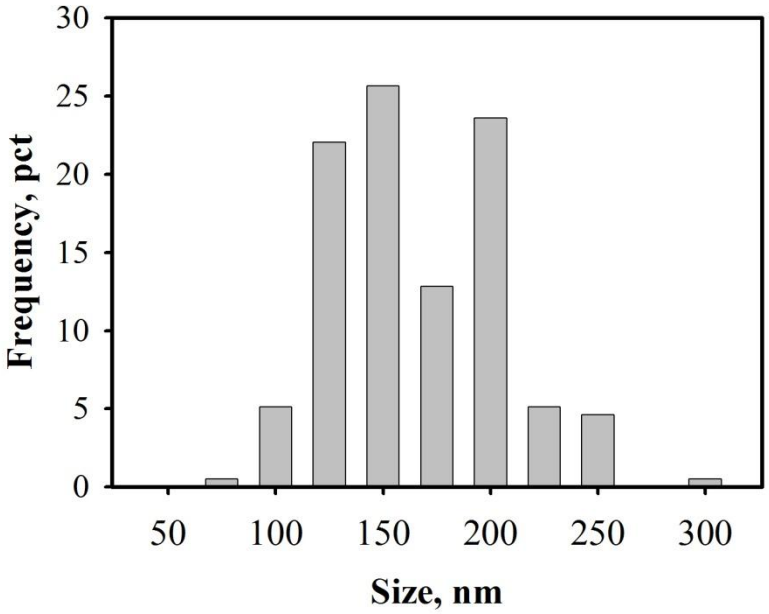

Figure 5-6: Carbide particles distribution for the 0.06C steel.

5.1.2 Austenite formation kinetics

The effect of heating rate on austenite formation has been quantified for the initial ferrite-carbide structure. The equilibrium (using Thermo-calc) and experimental (using dilation data) values of austenite volume fraction for the 0.06C steel and 0.12C steel are shown in Figure 5-7 and Figure 5-8, respectively. In ortho equilibrium the carbon as well as substitutional alloying additions redistribute relative to different steel phases whereas in the para equilibrium only carbon redistributes and the substitutional elements are configurationally frozen. The rate of austenite formation is higher for higher heating rates, i.e. for the 0.06C steel, it takes 150 seconds at 1^{o}C/s for complete transformation into austenite, whereas it takes only 1.5 seconds at 100^{o}C/s. In case of the 0.12C steel, this process takes 17 seconds at 10^{o}C/s and 1.6 seconds at 100^{o}C/s.

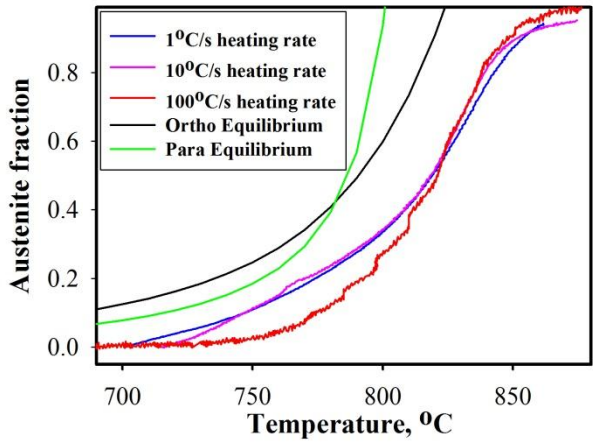

Figure 5-7: Austenite volume fraction vs. temperature graph for the 0.06C steel. The starting microstructure is ferrite-carbide aggregate.

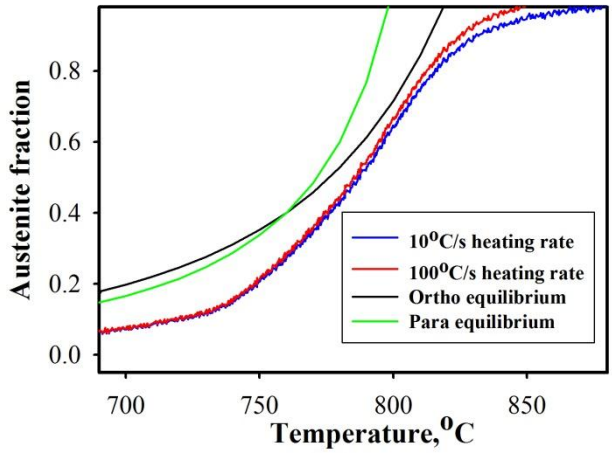

Figure 5-8: Austenite volume fraction vs. temperature graph for the 0.12C steel. The starting microstructure is ferrite-carbide aggregate.

The austenite start and finish temperatures are summarized in Table 5-1 for both the 0.06C and the 0.12C steels, where A_{e1} and A_{e3} are the ortho-equilibrium values and A_{c1} (at 0.05 fraction of austenite) and A_{c3} (at 0.95 fraction of austenite) are the experimental, start and finish temperatures upon heating, respectively. For the 0.06C steel, the heating rate has a significant effect on the start temperatures (i.e. the start temperature increases with heating rate) but not on the finish temperatures. On the other hand there is no effect of heating rate on the start and finish temperatures for the 0.12C steel. Moreover as the carbon content in the steel increases there is a

decrease in the start and finish temperatures. So to obtain the same desired volume fraction of martensite upon quenching, lower intercritical holding temperatures have to be employed for higher carbon as compared to lower carbon steels.

The goal is to obtain a volume fraction of martensite of approximately 0.2-0.25 upon quenching with a short holding time. Isothermal dilatometry tests were conducted for the 0.06C and the 0.12C steels to find the effect of holding time on the fraction of austenite formed during intercritical annealing. Dilation was measured for samples which were heated (at 10 and 100^{o}C/s) to the intercritical temperatures (750^{o}C for the 0.06C steel and 730^{o}C for the 0.12C steel) and held there for 30 seconds followed by continuous heating. The austenite fractions during intercritical holding time are shown in Figure 5-9 and Figure 5-10 for both the 0.06C and the 0.12C steels, respectively. In addition to dilation data the austenite fraction was also measured

Table 5-1: The austenite start and finish temperature values with heating rate for both the 0.06C and 0.12C steels. Ferrite-carbide aggregate is the starting microstructure

Steel	**0.06C**	**0.12C**
Ac_1, ºC, 1 ºC/s	700	-
Ac_3, ºC, 1 ºC/s	861	-
Ac_1, ºC, 10 ºC/s	715	688
Ac_3, ºC, 10 ºC/s	868	843
Ac_1, ºC, 100 ºC/s	751	690
Ac_3, ºC, 100 ºC/s	858	837
Ae_1, ºC	660	676
Ae_3, ºC	824	820

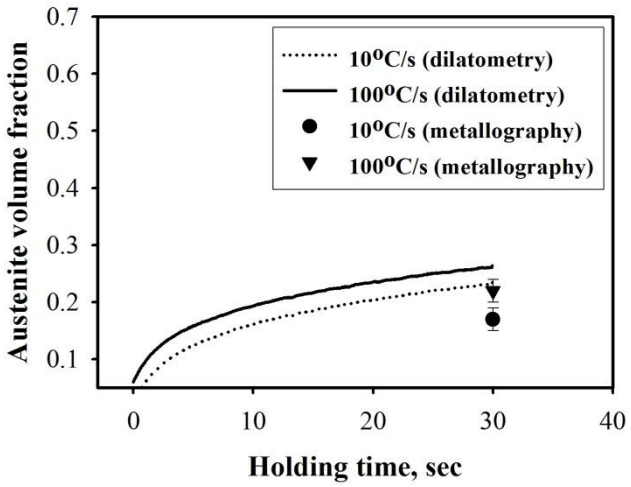

Figure 5-9: Evolution of austenite volume fraction during holding at 750°C for the 0.06C steel with a starting microstructure of ferrite-carbide aggregates.

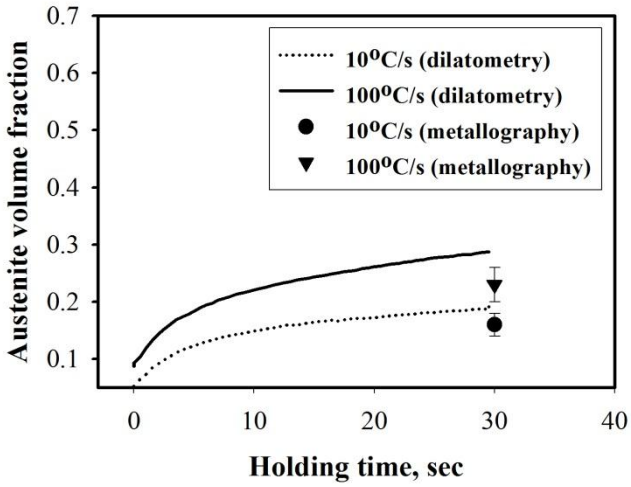

Figure 5-10: Evolution of austenite volume fraction during holding at 730°C for the 0.12C steel with a starting microstructure of ferrite-carbide aggregates.

metallographically for selected holding times using SEM micrographs. For both steels the austenite volume fractions are larger for the 100°C/s heating rate as compared to that of the 10°C/s heating rate. For the 0.12C steel the effect is significantly higher, i.e. the difference in volume fraction for the two heating rates is 0.1. Moreover the dilatometry values are higher than the metallography values for both steels irrespective of the heating rates. While analysing the

dilation data, the effect of carbon content on the lattice parameter is neglected during austenite formation. For low fractions (~0.2) of austenite formed the effect of carbon content on the lattice parameter is quite significant and this might have resulted in the high volume fraction values predicted by dilatometry as compared to metallography.

The effect of heating rate on austenite formation was also quantified for martensite starting microstructure. The graphs are shown in Figure 5-11 and Figure 5-12 for the 0.06C and 0.12C steels, respectively. Here also the rate of austenite transformation increases with heating rate. For the 0.06C steel, the time for the complete austenite transformation at 1^{o}C/s and 100^{o}C/s heating rates is 107 and 1.1 seconds, respectively whereas for the 0.12C steel, it is 100 and 1.1 seconds, respectively.

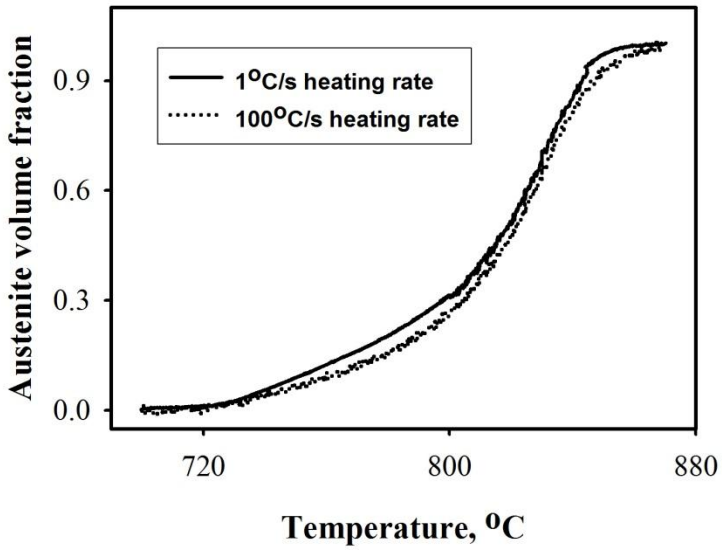

Figure 5-11: Austenite volume fraction vs. temperature graph for the 0.06C steel. The starting microstructure is martensite.

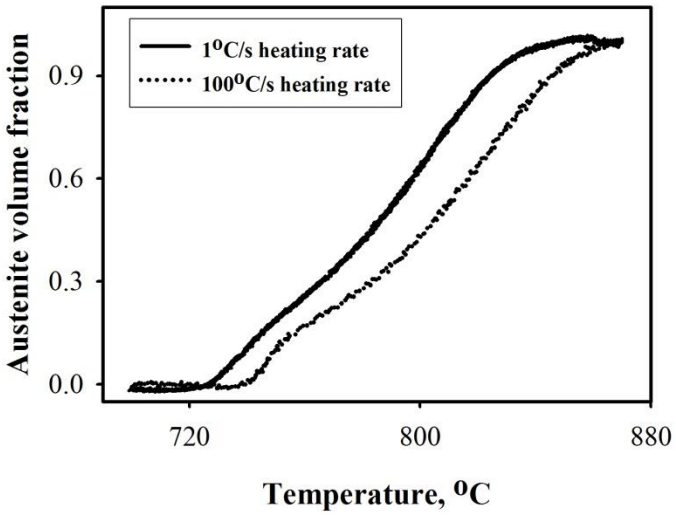

Figure 5-12: Austenite volume fraction vs. temperature graph for the 0.12C steel. The starting microstructure is martensite.

Table 5-2 summarizes the austenite start and finish temperatures as a function of heating rate. It can be seen that the effect of heating rate on critical temperatures in the 0.12C steel is more pronounced compared with the 0.06C steel.

Table 5-2: The austenite start and finish temperature values with heating rate for both the 0.06C and 0.12C steels. Matensite is the starting microstructure

Steel	**0.06C**	**0.12C**
Ac_1, ºC, 1 ºC/s	738	733
Ac_3, ºC, 1 ºC/s	845	832
Ac_1, ºC, 100 ºC/s	744	745
Ac_3, ºC, 100 ºC/s	853	852
Ae_1, ºC	660	676
Ae_3, ºC	824	820

Here also the aim is to obtain 0.2 volume fraction of martensite upon quenching. For the 0.06C steel the intercritical holding temperature is chosen at 780^{o}C for both the heating rates (as there is no effect of heating rate on the austenite fraction as a function of temperature) but for the 0.12C steel, the intercritical holding temperature is chosen at 750^{o}C for 1^{o}C/s heating rate and 760^{o}C for the 100^{o}C/s heating rate.

5.1.3 Microstructure and mechanical properties of DP structures formed using ferrite-carbide aggregates

The fine ferrite-carbide aggregate structure was used as the initial structure for intercritical annealing. The holding temperature for intercritical annealing was 750^{o}C for the 0.06C and 730^{o}C for the 0.12C steel. The UFG DP microstructures are shown in Figure 5-13. Here the heating rate was 100^{o}C/s and helium was used as the quenching medium. The inset in Figure 5-13 provides a higher magnification image of the DP structure. The martensite islands are very fine (0.3 μm and 0.45 μm for the 0.06C and 0.12C steel, respectively) with a banded structure.

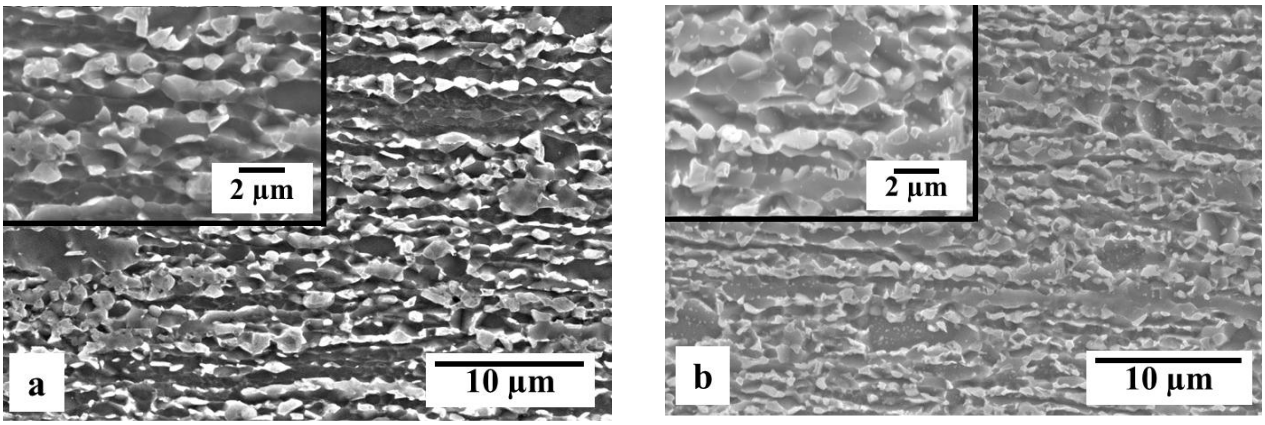

Figure 5-13: UFG DP structures obtained using fine ferrite-carbide aggregate heated at 100^{o}C/s (a) the 0.06C steel, holding temperature is 750^{o}C and (b) the 0.12C steel, holding temperature is 730^{o}C. Higher magnification images are shown as inset.

For the 0.06C steel, as the heating rate increases from 1°C/s to 100°C/s, the microstructure is finer and the area fraction of the martensite is higher, see Figure 5-14.

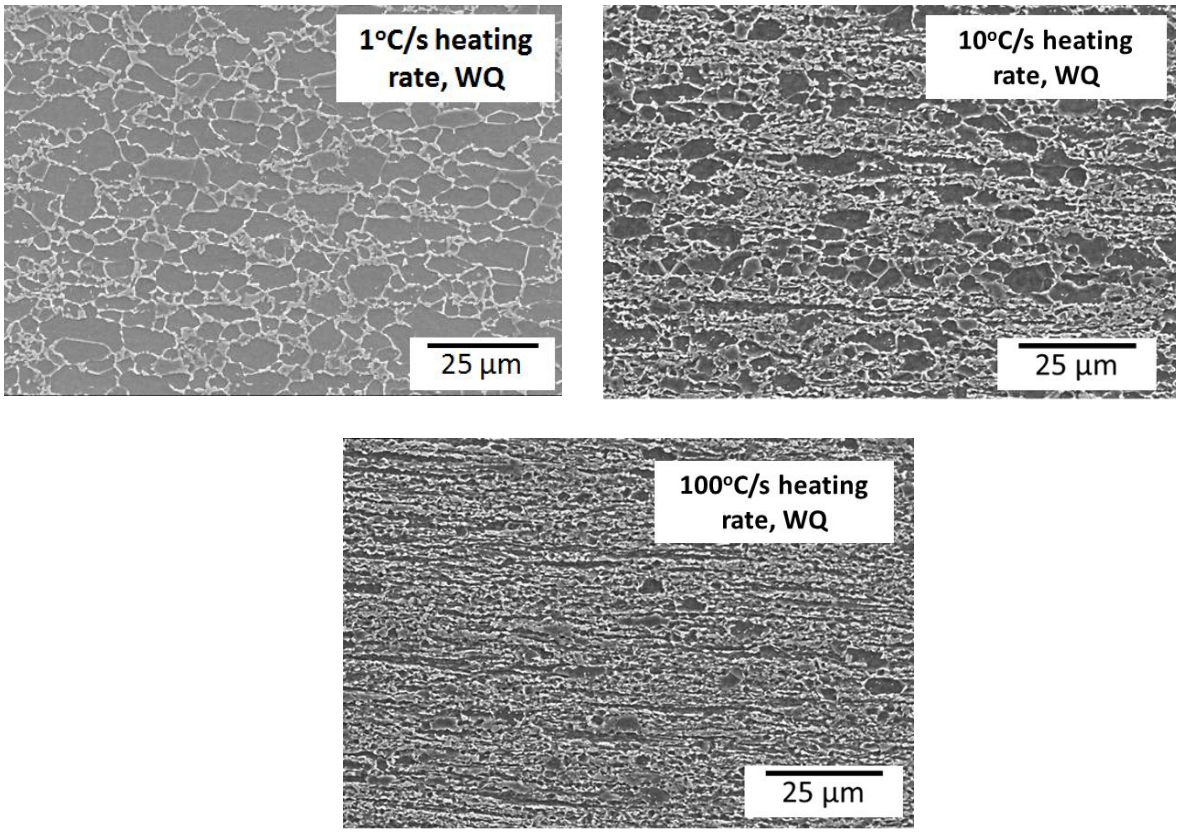

Figure 5-14: Effect of heating rate on the final DP microstructure of the 0.06C steel. Annealing temperature is 750°C with 30 seconds holding time and quenched using water. The starting microstructure is ferrite-carbide (WQ: water quenching).

As the heating rate increases, the microstructure tends to change from equiaxed to banded morphology. The number density of coarse grains increases with decreasing heating rate. For 1°C/s heating rate the microstructure is much coarser compared to higher heating rates, thus no further studies were conducted for the 1°C/s heating rate conditions. The size distribution of martensite islands is shown in Figure 5-15 for 10°C/s and 100°C/s in the 0.06C steel. The average martensite island size for 10°C/s and 100°C/s heating rates is 0.55 µm and 0.3 µm, respectively. The volume fraction of martensite for 10°C/s heating rate measured using the

isothermal dilatometry data and from metallography is found to be 0.23 and 0.17, respectively, whereas for 100°C/s heating rate a higher martensite volume fraction is observed, i.e. 0.27 and 0.22, respectively. In both cases, the metallographically obtained fraction is about 15% smaller than that measured using dilatometry.

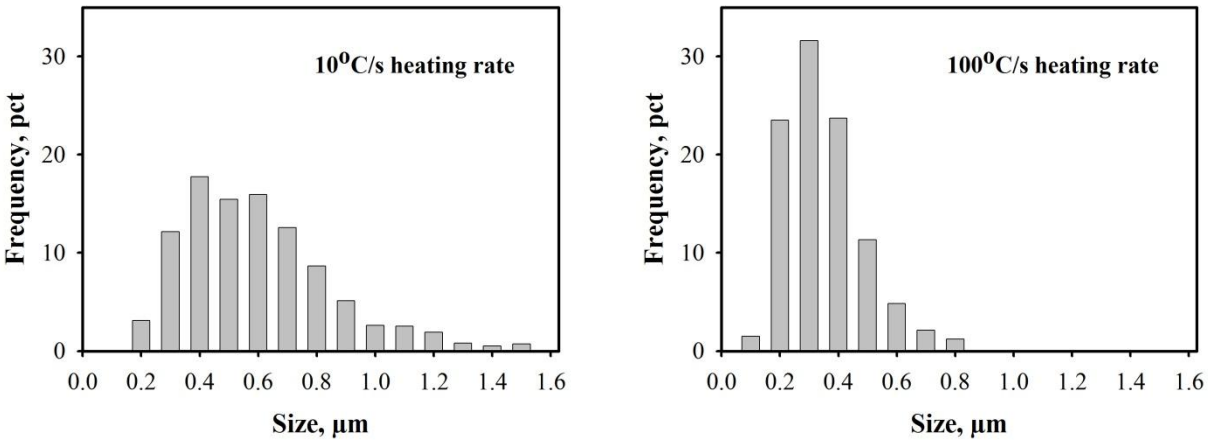

Figure 5-15: Effect of heating rate on the size distribution of martensite islands for the 0.06C DP structure. The starting microstructure is ferrite-carbide.

The effect of heating rate on the DP structures for the 0.12C steel is shown in Figure 5-16. Here, similar to the 0.06C steel, with an increase in the heating rate the microstructure tends to be finer and the morphology changes from equiaxed to banded. In case of the 1°C/s heating rate the DP structure is coarser compared to the higher heating rates and moreover there is no significant presence of martensite phase, hence no further studies have been conducted. The size distribution of martensite islands is shown in Figure 5-17 for 10°C/s and 100°C/s heating rate for the 0.12C steel. The average martensite island size for 10°C/s and 100°C/s heating rates are 0.56 µm and 0.45 µm, respectively. The volume fraction of martensite for 10°C/s heating rate measured using the isothermal dilatometry data and by metallography is found to be 0.18 and 0.16, respectively, whereas for the higher heating rate of 100°C/s a higher martensite volume fraction is observed,

i.e. 0.26 and 0.23, respectively. Here also the dilation data suggests a higher volume fraction as compared to the metallography analysis.

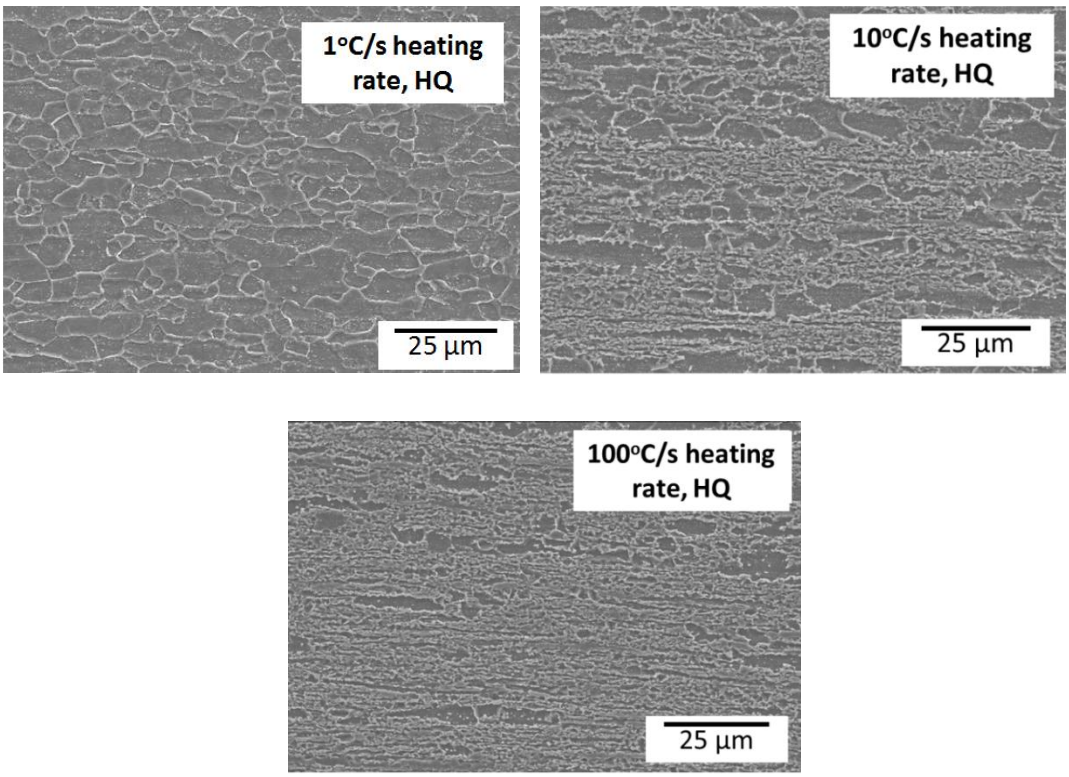

Figure 5-16: Effect of heating rate on the final DP microstructure of the 0.12C steel. Annealing temperature is 750°C with 30 seconds holding time and quenched using helium. The starting microstructure is ferrite-carbide (HQ: helium quenching).

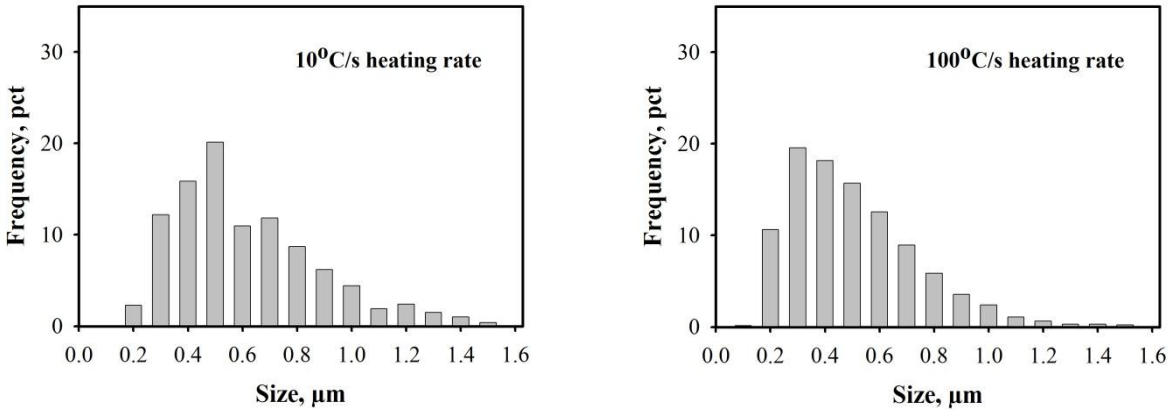

Figure 5-17: Effect of heating rate on the size distribution of martensite islands for the 0.12C DP structure. The starting microstructure is ferrite-carbide.

The effect of cooling rate on the final DP microstructure was studied for the 0.06C steel (see Figure 5-18). There is no difference in the microstructure in terms of grain size, but in terms of volume fraction of martensite there is a small difference i.e. 0.22 for higher cooling rate and 0.2 for lower cooling rate.

The effect of heating and cooling rates on the engineering stress-strain curve for the 0.06C steel is shown in Figure 5-19 and Figure 5-20, respectively. For higher heating rates (100^{o}C/s) both the UTS and the uniform elongation (UE) are higher as compared to the lower heating rate (10^{o}C/s) irrespective of the cooling rate (see Table 5-3). For higher cooling rate, the UTS is higher and the uniform elongation is lower as compared to the lower cooling rate. The heating and the cooling rates do not have a significant effect on the value of yield strength (YS) and yield ratio. The strength-elongation balance (UTS × UE) is the highest and the fracture strain is at least two times greater for 100^{o}C/s heating with 160^{o}C/s cooling rate as compared to the other two cases. A transition to a discontinuous yielding is also observed with a decrease in the cooling rate from 1000 to 160^{o}C/s.

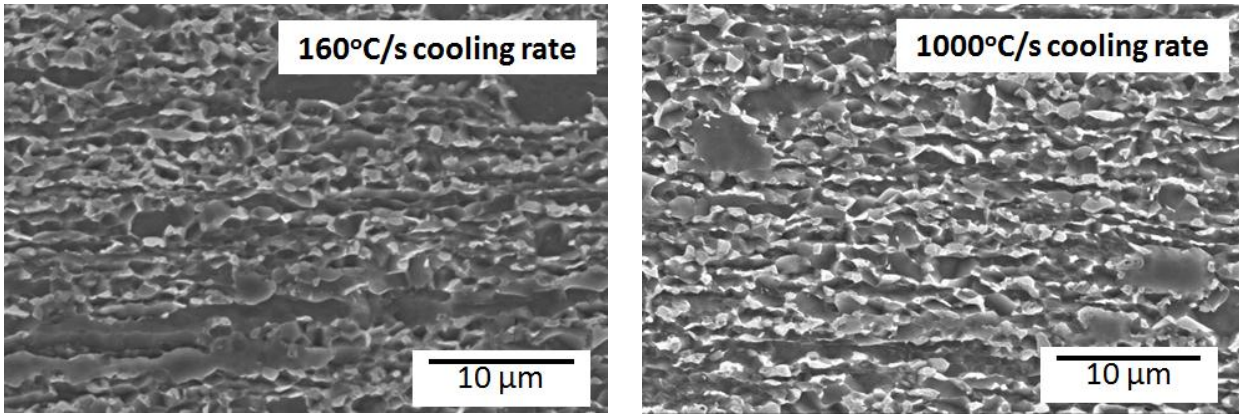

Figure 5-18: Effect of cooling rate on the final DP microstructure of the 0.06C steel. Annealing temperature is 750^{o}C with 100^{o}C/s heating rate and 30 seconds holding time. The starting microstructure is ferrite-carbide.

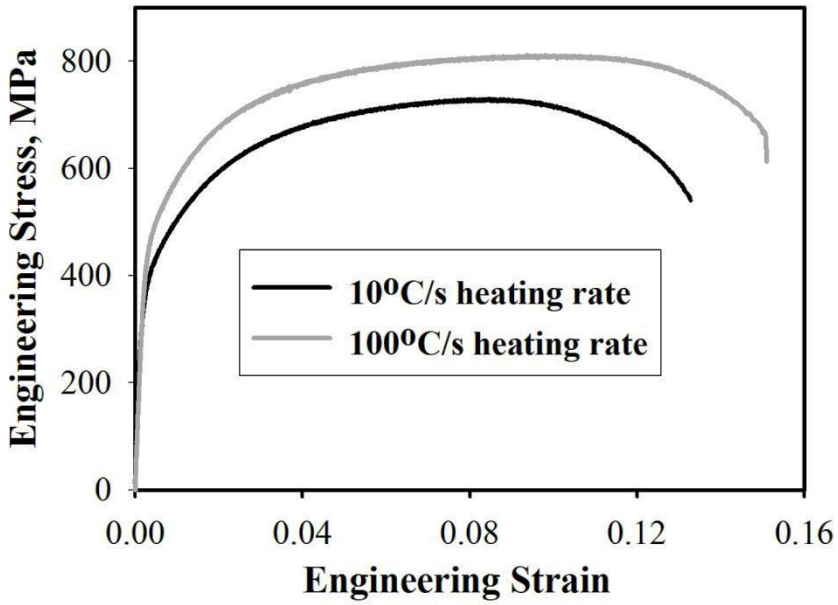

Figure 5-19: Effect of heating rate on the engineering stress strain curve for the 0.06C steel with ferrite-carbide starting microstructure. The cooling rate from the intercritical region is 1000°C/s.

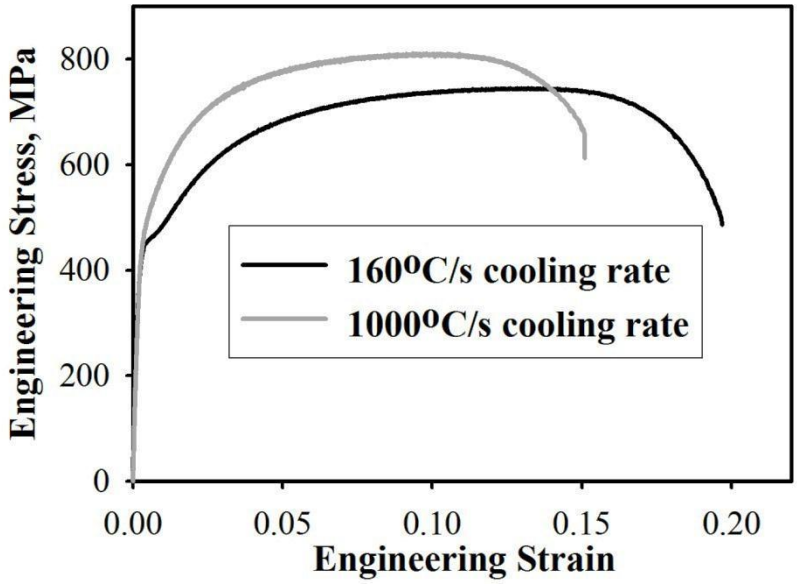

Figure 5-20: Effect of cooling rate on the engineering stress strain curve for the 0.06C steel. The starting microstructure is ferrite-carbide and the heating rate is 100°C/s.

Table 5-3: Effect of heating/cooling rates on the mechanical properties of the 0.06C steel with ferrite-carbide starting microstructure

Heating rate (^{o}C/s)	Cooling rate (^{o}C/s)	YS (0.2 pct offset), MPa	UTS, MPa	UE, pct	Total elongation (TE), pct	Fracture strain	Yield ratio	UTS×UE, MPa×pct
10	1000	402±4	728±3	8.6±0.1	13.5±0.1	0.69±0.07	0.55±0.01	6210±87
100	1000	464±7	802±9	9.4±0.4	14.5±0.6	0.57±0.04	0.58±0.01	7542±388
100	160	417±3	743±2	13.4±0.1	19.5±0.2	1.32±0.06	0.56±0.008	9918±84

The thickness of the fracture surface is significantly lower (at least 2 times) for the lower cooling rate as compared to the higher cooling rate (see Figure 5-21, the arrows in the figure show the thickness of the fracture surface). But there is no difference in the dimple size of the fracture micrograph for both the cooling rates.

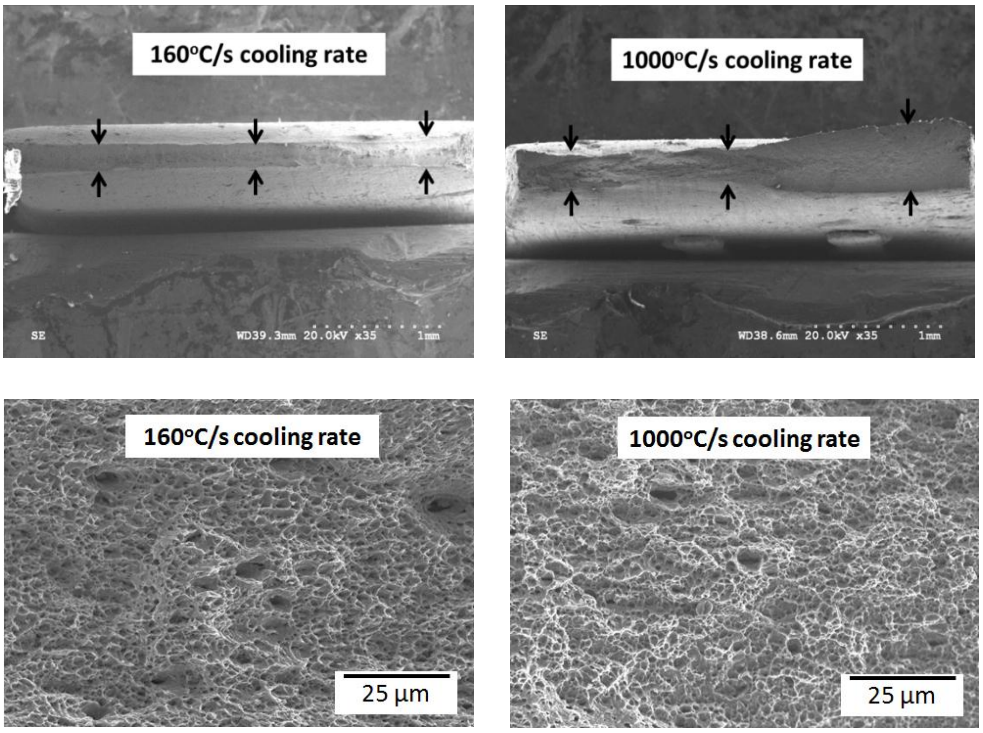

Figure 5-21: Effect of cooling rate on the fracture micrographs for the 0.06C steel. The starting microstructure is ferrite-carbide. The arrows show the thickness of the fracture surface (Intial cross-section was the same for both the samples).

In the case of the 0.12C steel, the stress-strain graph shows that for higher heating rate (100^{o}C/s) the UTS is higher but there is a decrease in the uniform elongation as compared to the lower heating rate (10^{o}C/s) (see Figure 5-22). The results are tabulated in Table 5-4. For the lower

heating rate (10°C/s) the yield strength and UTS are lower by 105 MPa and 91 MPa, respectively and the uniform and total elongation are higher by 2.4 pct and 2.2 pct, respectively as compared to the higher heating rate (100°C/s). The yield ratio values increases from 0.52 to 0.58 when the heating rate is increased from 10 to 100. Interestingly, there is no significant effect of heating rate on the strength-elongation balance, although lower heating rate has slightly higher strength-elongation values.

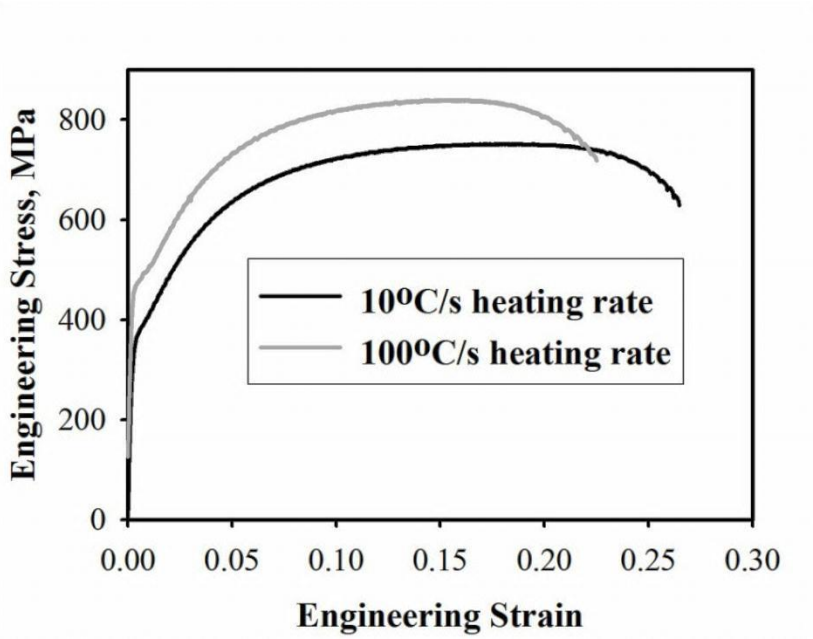

Figure 5-22: Effect of heating rate on the engineering stress strain curve for the 0.12C steel. The starting microstructure is ferrite-carbide.

Table 5-4: Effect of heating rate on the mechanical properties of the 0.12C steel with ferrite-carbide starting microstructure

Heating rate (°C/s)	YS (0.2 pct offset), MPa	UTS, MPa	UE, pct	Total elongation (TE), pct	Fracture strain	Yield ratio	UTS×UE, MPa×pct
10	385±15	751±1	17.4±0.5	25.2±0.8	0.63±0.03	0.52±0.02	13102±357
100	490±4	842±2	15±0.1	23±0.5	0.60±0.02	0.58±0.01	12672±12

5.1.4 Microstructure and properties of DP structures formed using martensite microstructure

Martensite was also used as the starting microstructure so as to compare the effect of starting microstructure on the final microstructure and mechanical properties of DP steel. The effect of heating rate on the microstructure is shown in Figure 5-23 for the 0.06C steel. The martensite phase is predominantly lath microstructure which is in contrast to the equiaxed martensite phase that is obtained using the ferrite-carbide aggregates structure. As the heating rate increases from 1^{o}C/s to 100^{o}C/s, there is a decrease in the number density of coarse ferrite grains.

The size distribution of martensite islands for the 0.06C DP steel is shown in Figure 5-24. The average martensite island size for 1^{o}C/s and 100^{o}C/s heating rates are 0.72 μm and 0.74 μm, respectively. The volume fraction of martensite for 1^{o}C/s heating rate measured using the dilatometry data and metallography is found to be 0.20 and 0.15, respectively, and for the higher heating rate of 100^{o}C/s a similar volume fraction is observed, i.e. 0.18 and 0.15, respectively.

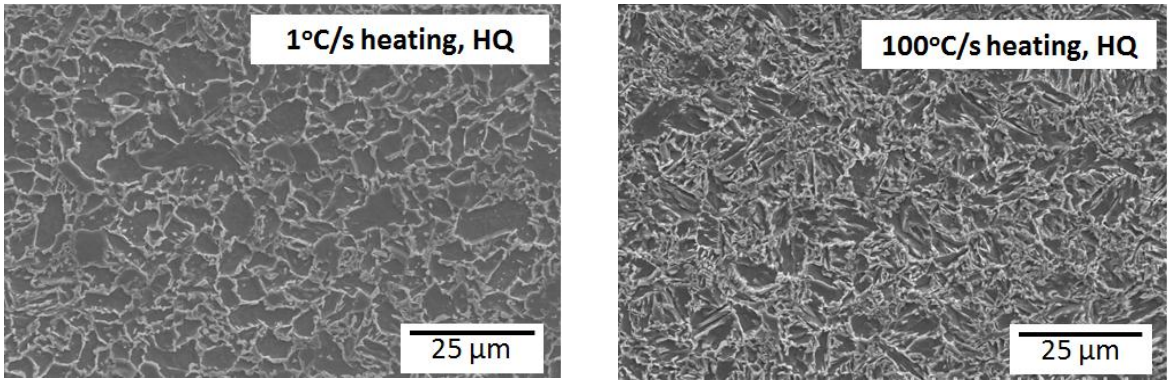

Figure 5-23: Effect of heating rate on the final DP microstructure of the 0.06C steel. Annealing temperature is 780^{o}C with 30 seconds holding time and quenched using helium. The starting microstructure is martensite.

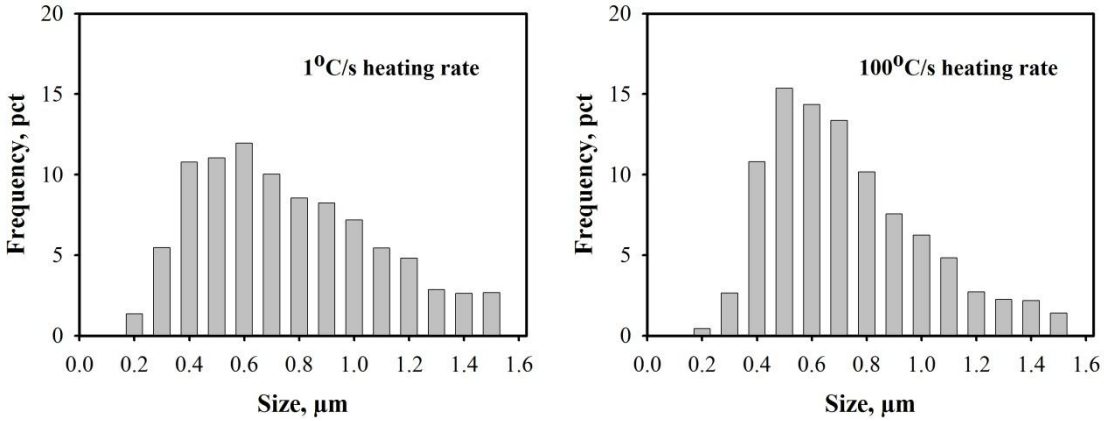

Figure 5-24: Effect of heating rate on the size distribution of martensite islands for the 0.06C DP structure. The starting microstructure is martensite.

A similar microstructural behavior was observed for the 0.12 C steel as well, see Figure 5-25. Increasing the heating rate leads to finer microstructure. The size distribution of martensite islands for 1°C/s and 100°C/s heating rates for the 0.12C steel using martensite as the starting microstructure is shown in Figure 5-26. The average martensite island size for 1°C/s and 100°C/s heating rates are 0.82 µm and 0.72 µm, respectively. The volume fraction of martensite for 1°C/s heating rate measured using the dilatometry data and metallography is found to be 0.26 and 0.24 respectively, and similar volume fractions are also observed for the higher heating rate of 100°C/s, i.e. 0.25 and 0.23, respectively.

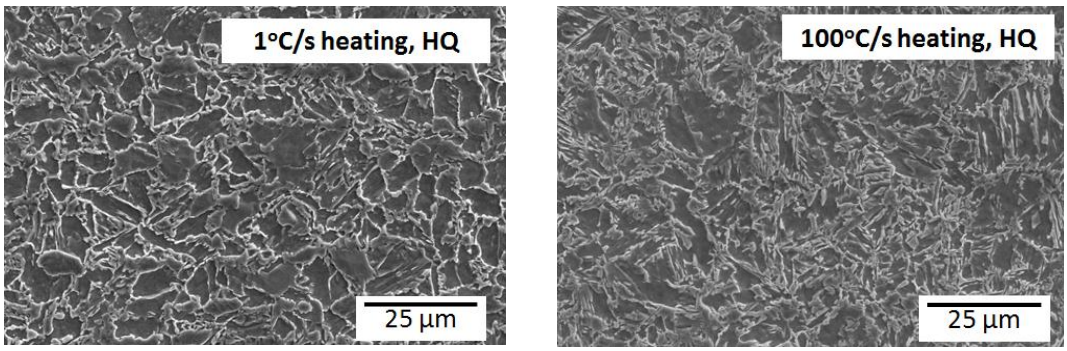

Figure 5-25: Effect of heating rate on the final DP microstructure of the 0.12C steel. Annealing temperature is 750°C for 1°C/s heating rate and 760°C for 100°C/s heating rate, with 30 seconds holding time followed by helium quenching. The starting microstructure is martensite.

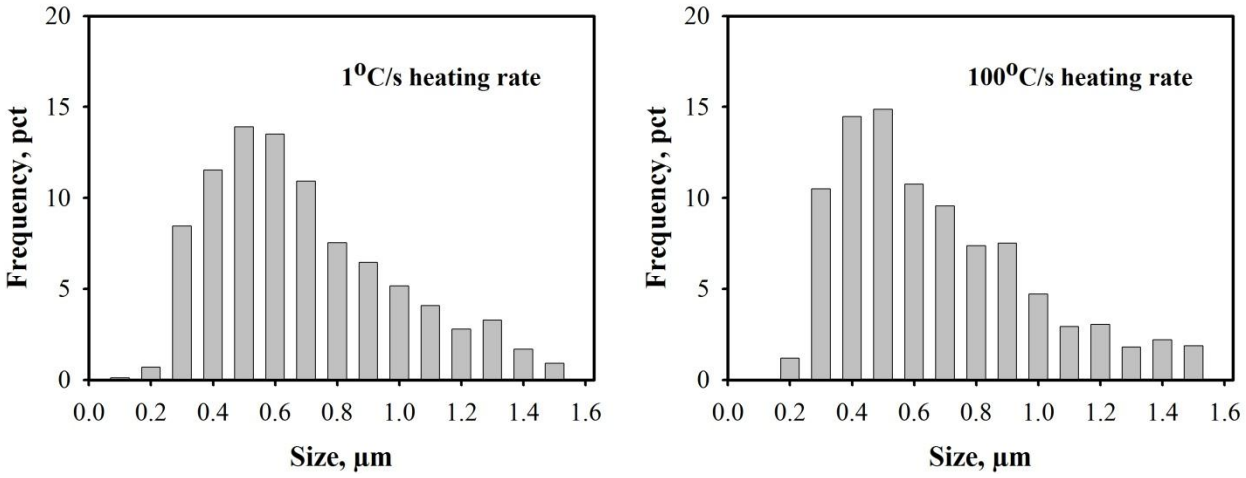

Figure 5-26: Effect of heating rate on the size distribution of martensite islands for the 0.12C DP structure. The starting microstructure is martensite.

For the 0.06C steel, the effect of heating rate on the stress-strain behavior is plotted in Figure 5-27. There is no significant effect of heating rate on the UTS, YS and UE values. Hence there was no effect on the yield ratio as well as the strength-elongation balances. There is a slight effect on the TE and fracture strain values, i.e. higher heating rate promotes better TE and fracture strain values (refer to Table 5-5).

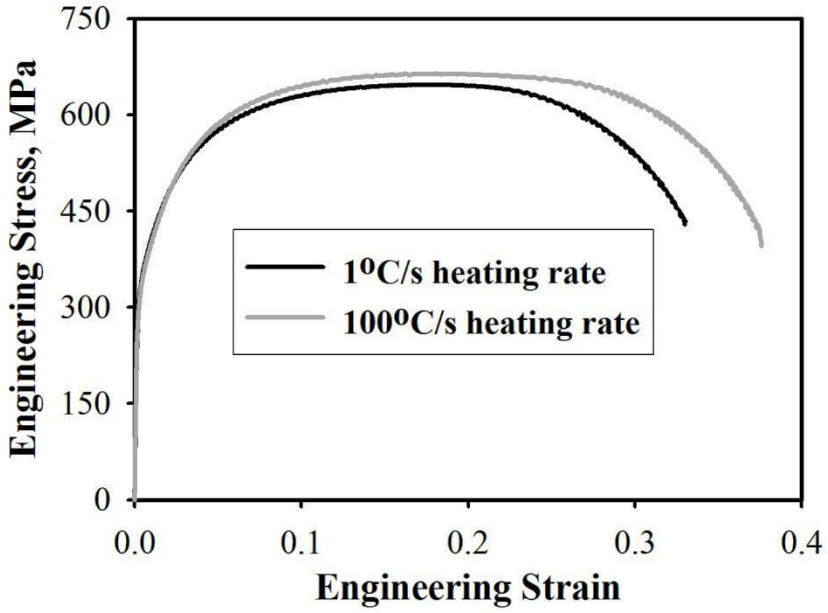

Figure 5-27: Effect of heating rate on the engineering stress strain curve for the 0.06C steel. The starting microstructure is martensite.

Table 5-5: Effect of heating rate on the mechanical properties of the 0.06C steel with martensite starting microstructure

Heating rate (°C/s)	YS (0.2 pct offset), MPa	UTS, MPa	Uniform Elongation (UE), pct	Total Elongation (TE), pct	Fracture strain	Yield ratio	UTS×UE, MPa×pct
1	335±3	648±1	17.5±0.5	32.7±0.3	1.12±0.03	0.51±0.01	11331±315
100	330±10	665±1	17.4±0.6	35±3	1.27±0.03	0.5±0.01	11562±390

The effect of the heating rate on the engineering stress-strain curve for the 0.12C steel is shown in Figure 5-28.

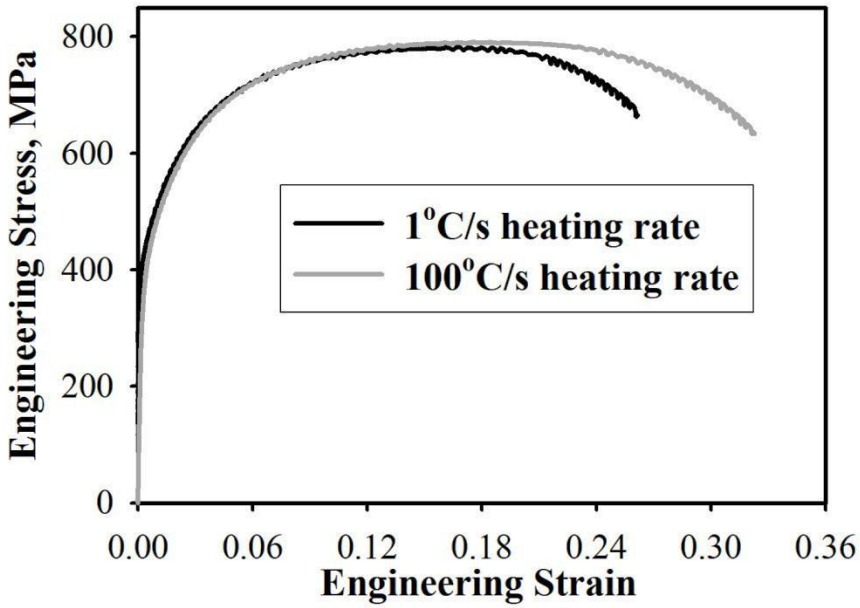

Figure 5-28: Effect of heating rate on the engineering stress strain curve for the 0.12C steel. The starting microstructure is martensite.

There is no significant effect of heating rate on the YS and UTS but for higher heating rates (100^{o}C/s) the uniform elongation is higher as compared to the lower heating rates (1^{o}C/s). For higher heating rate (100^{o}C/s) the uniform and total elongation are increased by 2.5 pct and 8.3 pct, respectively as compared to the lower heating rate (1^{o}C/s) (see Table 5-6). Since there is no significant difference in the UTS and yield strength values, there is also no change in the yield ratio. The fracture strain at 100^{o}C/s heating rate is greater by about 0.26 as compared to the lower heating rate (1^{o}C/s) and this difference in the fracture strain value is evident from the fracture micrograph (see Figure 5-29, the arrows point to the thickness of the fracture surface). There is a significantly reduced width of the fracture surface for higher heating rate (100^{o}C/s). The microstructure of the fracture surface reveals that for 100^{o}C/s the dimple size is finer

compared to the 1°C/s heating rate, which implies that the energy absorbed during deformation is higher for 100°C/s heating rate.

Table 5-6: Effect of heating rate on the mechanical properties of the 0.12C steel with martensite starting microstructure

Heating rate (°C/s)	YS (0.2 pct offset), MPa	UTS, MPa	Uniform Elongation (UE), pct	Total Elongation (TE), pct	Fracture strain	Yield ratio	UTS×UE, MPa×pct
1	440±40	804±21	15.8±0.9	25.6±0.6	0.45±0.04	0.55±0.04	12676±384
100	386±4	769±21	18.3±0.7	33.9±1.6	0.72±0.03	0.50±0.01	14058±125

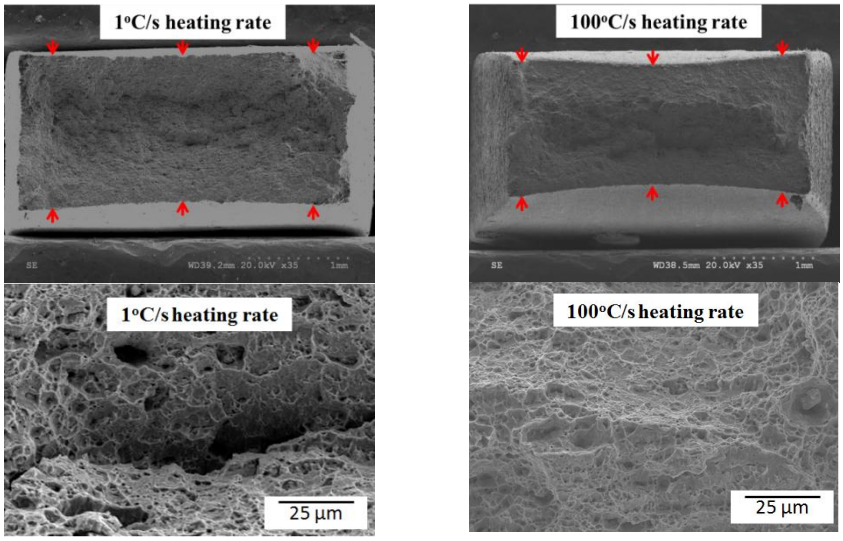

Figure 5-29: Effect of cooling rate on the fracture micrographs for the 0.12C steel. The starting microstructure martensite. The arrows point the thickness of the fracture surface (Intial cross-section was the same for both the samples).

5.2 Mo and Nb containing plain carbon steels

To potentially reduce the heating and cooling rates in the proposed rapid intercritical annealing treatment it is of interest to form DP structures using ferrite-carbide aggregates in micro-alloyed steels. Two different low carbon steels containing small additions of Mo and Nb were used for this investigation. Ferrite-pearlite is the starting microstructure for both the steels, as shown in Figure 5-30. Ferrite is the dark grey area and pearlite appears as lighter area with a characteristic lamellar structure in the micrograph. Ferrite grains are equiaxed in the Nb containing steels but

they are preferentially oriented along the rolling direction in the Mo containing steel, since this steel had been received in a cold-rolled condition (55 pct cold reduction). The Mo steel in the as-received state and the Nb steel, which was cold-rolled (by 75 pct) to 4mm thickness, were austenitized at 950^{o}C for 10 minutes, followed by water quenching to room temperature to obtain martensite. Lath type morphology is predominantly present in the martensite phase for both the steels.

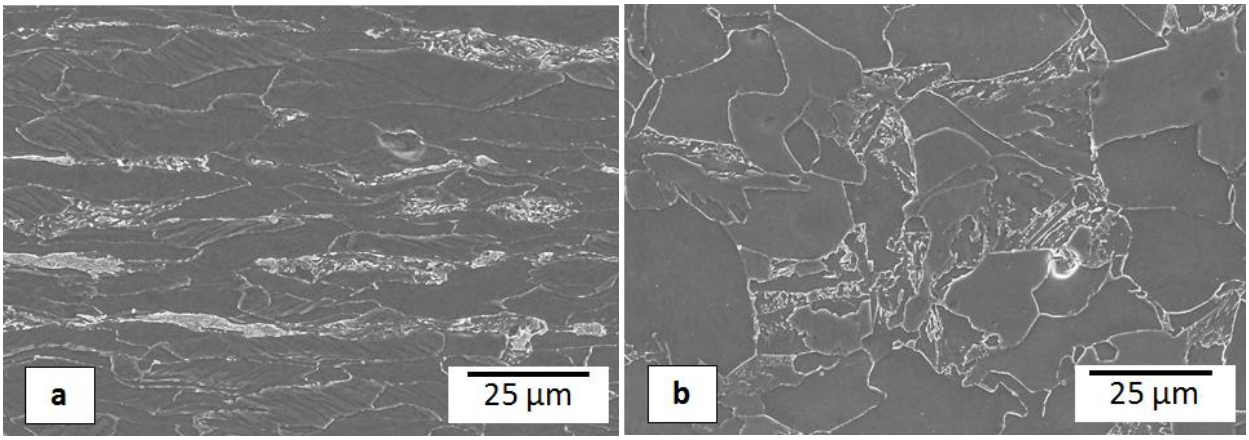

Figure 5-30: Initial ferrite-pearlite microstructures of (a) Mo and (b) Nb containing steels.

To soften the martenstie phase prior to cold-rolling a tempering step at 550^{o}C for 1h was used to obtain a tempered martensite structure, shown in Figure 5-31. The Vickers hardness for the martensite structure is 364HV and 352HV for the Mo and Nb containing steels, respectively, whereas for the tempered martensite structure there is a significant drop of over 100HV to 242HV and 238HV, respectively. Similar to the plain carbon steels fine carbide particles are predominantly found at the lath and prior austenite grain boundaries in the micro-alloyed steels.

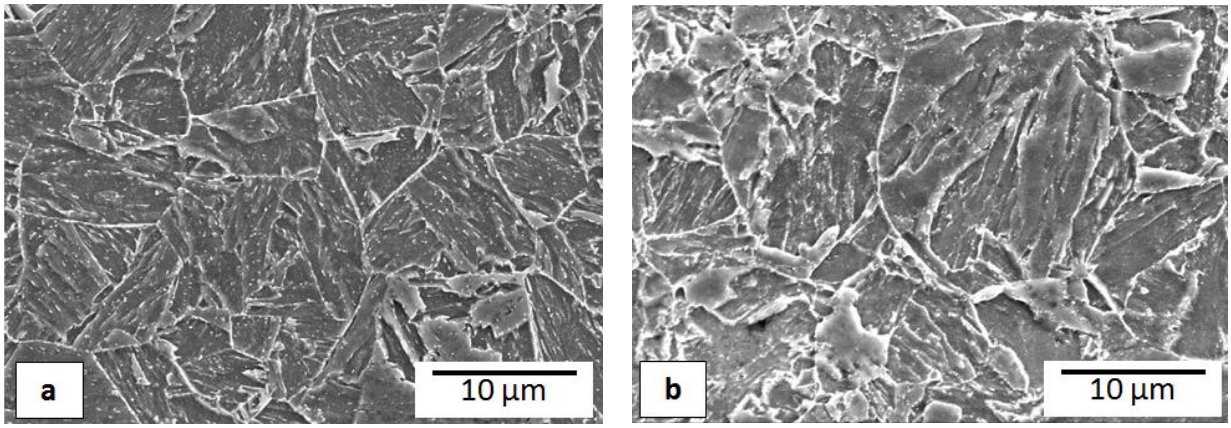

Figure 5-31: Tempered martensite structure of (a) Mo and (b) Nb containing steels.

The tempered martensite structure was subsequently 80 pct cold rolled to obtain cold-rolled tempered martensite structure. An additional tempering step at 550^{o}C for 1 h was performed with the aim to obtain recrystallized fine ferrite-carbide aggregates, but for both the Mo and Nb containing steels the ferrite is non-recrystallised and moreover there were no coarse carbide particles observed, see Figure 5-32. Since the microstructure was still not recrystallized, tempering time and temperature were varied in an attempt to obtain recrystallized fine ferrite-carbide aggregates. Increasing the tempering temperature (1h at 600^{o}C) lead to the formation of coarse ferrite-carbide aggregates for both the steels.

Thus, an additional warm rolling approach has been implemented on the tempered martensite structure for Mo containing steel (see Figure 5-31) with the goal to obtain fine ferrite-carbide aggregate. The tempered martensite structure of the Mo containing steel was held for 10 min at 650^{o}C and 700^{o}C, respectively, and then immediately rolled. The microstructures obtained after holding at 650^{o}C is shown in Figure 5-33. The warm rolling approach has also failed to obtain a fine ferrite-carbide aggregates structure in the Mo containing steel. Hence, the proposed

processing route failed to create fine ferrite-carbide aggregates in micro-alloyed steels and hence new processing routes have to be developed to address this issue.

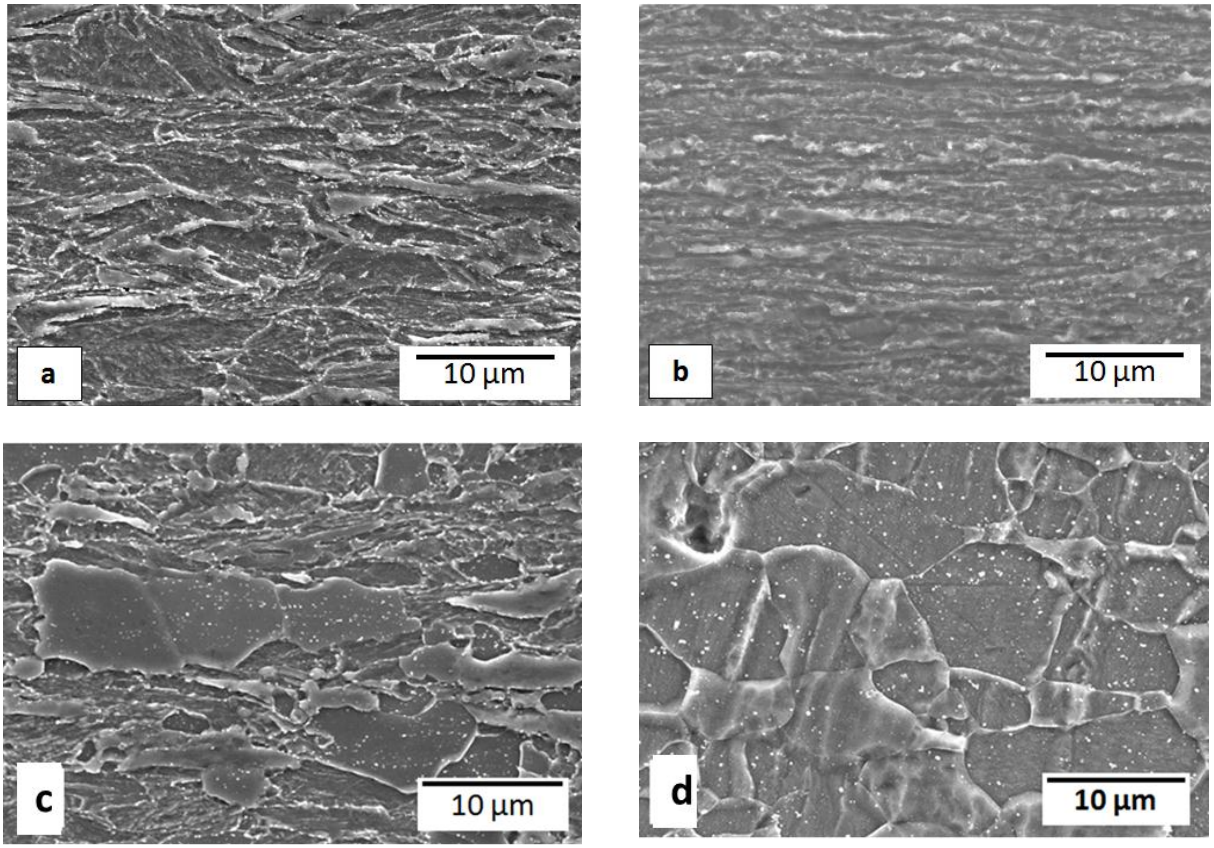

Figure 5-32: Ferrite-carbide aggregates obtained after tempering for 1hr at 550^{o}C [(a) Mo and (b) Nb], and, 1hr at 600^{o}C [(c) Mo and (d) Nb].

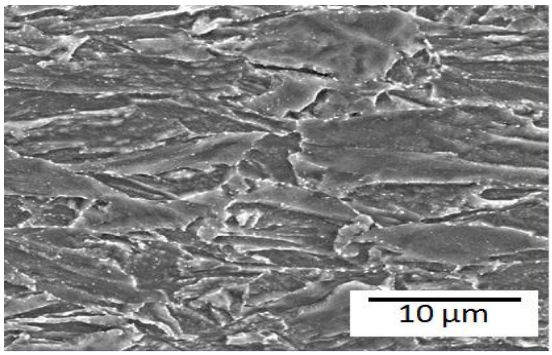

Figure 5-33: Tempered martensite structure of Mo containing steel held for 10 min at 650^{o}C and immediately rolled.

6 Discussion

6.1 Plain carbon steels

6.1.1 Austenite formation kinetics

The continuous heating transformation data indicates an increase in the rate of austenite formation by about a factor of 100 when increasing heating rate from 1 to 100^{o}C/s. Hence isothermal holding tests were performed to quantify the effect of heating rate on the amount of austenite formed for a particular intercritical temperature, which yielded two important findings: firstly, the amount of austenite formed increases with holding time, as expected. Secondly, the more interesting observation is that the samples with higher heating rates have a much higher austenite volume fraction for a given annealing time. The amount of austenite formed during the intercritical holding time is tabulated in Table 6-1. It can be seen that for both steels, the fraction of austenite formed during holding after heating at 100^{o}C/s is about 50% higher than for heating at 10^{o}C/s, even with similar amounts of austenite to start with.

Table 6-1: Effect of heating rate on the fraction of austenite formed during 30 seconds holding time. Ferrite-carbide is the starting microstructure

Steel	**0.06C**	**0.12C**
10^{o}C/s	0.1	0.13
100^{o}C/s	0.15	0.18

This is due to the change in the initial structure at the onset of austenite formation with heating rate, i.e. there is much more ferrite grain growth during slow heating hence coarser ferrite grains for lower heating rates as compared to the higher heating rate. In part this is also due to the competition of nucleation and growth, which is explained by Huang et al. [63]. The austenite transformation starts from the carbide particles by nucleation at the carbide-ferrite interface

followed by quick growth consuming the dissolving carbide particles. Subsequently, austenite may nucleate at ferrite grain boundaries in competition with austenite growth from the prior carbide particles at the carbide-ferrite interface. It appears that the competition between austenite formed at these different sites is responsible for the marked heating rate effect on the transformation kinetics. Slower heating rates will favor substantial growth of austenite nucleated from carbide particles, whereas faster heating rates will promote additional nucleation at ferrite grain boundaries. This explanation is consistent with the metallographical observations made in the current work, which revealed that the grain size of martensite becomes finer with increasing heating rate, and also the presence of coarse ferrite grains for lower heating rates. The number density of martensite islands is also higher for higher heating rates for a given area.

6.1.2 Mechanical properties

UTS and UE play a key role in the design of automotive steels. Increasing the strength (UTS) helps in reducing the gauge (thickness) of the sheet, thereby reducing the weight (for fuel efficiency) and amount of material used (reducing material cost). Increased UE is important to conduct complex stamping operations. Hence UTS-UE balance is of significant importance in the evaluation of DP steels. Thus, a graph of UTS vs. UE has been plotted to compare the UFG DP steels developed in this study with the coarse grained (CG) and UFG DP steels from the literature, see Figure 6-1. The steels shown in this representation are low carbon (varies between 0.05-0.20 wt pct) steels containing less than 2 wt pct Mn and less than 1 wt pct of other alloying additions. The martensite volume fraction ranges between 0.15-0.35. The dotted trend line indicates the upper limit values of the UFG DP steels and the solid trend line indicates the upper limit values of the coarse grain DP steels. The filled squares represent the 0.12C steel and the

filled triangles represent the 0.06C UFG DP steels used in this study. The filled circles represent the UFG DP steels and the open circles represent the coarse grained DP steels from literature.

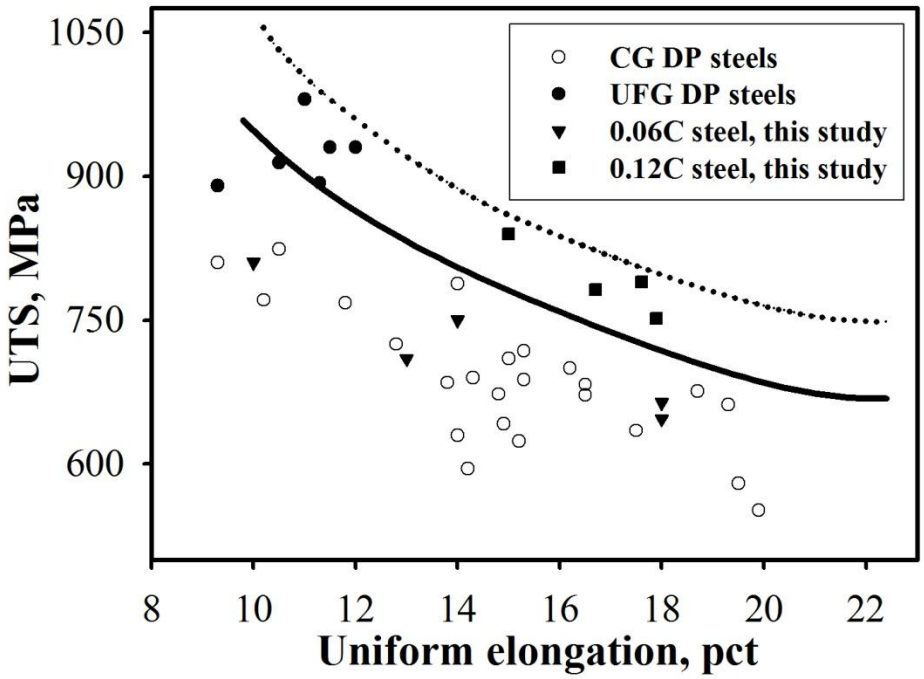

Figure 6-1: Comparison of UTS vs. UE for various DP steels [5, 7, 9, 10, 21, 39, 59, 61, 64].

The CG DP steels fall below the solid curve and the UFG DP steels expand the property combination to the dashed line indicating that for a given UE, the UFG DP steels can have about 100 MPa higher UTS as compared to their coarse grained counterparts. The 0.12C UFG DP steels developed in this study followed a similar trend as the UFG DP from literature, but in a range of lower UTS but higher UE. In the case of the 0.06C steel, it was expected that they follow a similar trend, but this was not the case.

For a given volume fraction of martensite, an increase in the carbon content of steel results in an increase in the UTS and this is accompanied by a reduction in UE because of higher carbon content in the martensite [9] which explains the higher UTS and lower UE values observed for the UFG DP steels from the literature (with carbon content $\geq$ 0.17 wt pct) as compared to the

UFG DP steels used in this study. It also explains the significantly lower UTS values for the 0.06C steel as compared to other UFG DP steels. It is expected that this low UTS value would yield higher UE values, but this was not observed for the 0.06C steel. To summarize, in the present study it was found that the carbon content plays a significant role in obtaining a desired UTS-UE balance, and below a critical carbon level, the decrement in UTS will not be complemented with an increment in UE values. Further work must be done on various lower carbon DP steels to verify this finding.

Considering processing of these UFG DP steels, Park et al. [59] used equal channel angular processing (ECAP) for fabrication, which is very cumbersome (if not impossible) to employ in a commercial steel processing line. Calcagnotto et al. [64] used warm deformation, which is again not very promising due to huge deformation induced at higher temperatures. The route proposed by Azizi-Alizamini et al. [7] seems to be promising for sheet production of DP steels but they employed very high heating and cooling rates (300^{o}C/s and 1000^{o}C/s, respectively) to achieve an improvement in the mechanical properties over the CG DP steels. In the present study, while using the approach of Azizi-Alizamini et al. [7], the UFG DP structures (0.12C) were fabricated by employing lower heating (1, 10 and 100^{o}C/s) and cooling rates ($< 300^{o}$C/s) to achieve similar improvements of the UTS-UE balance.

The previous studies conducted to fabricate UFG DP steels consisted of multiple steps prior to intercritical annealing, but using martensite as the starting microstructure for intercritical annealing will significantly reduce the number of processing steps. Moreover, the mechanical properties obtained using martensite starting structures are comparable to the ones obtained using ferrite-carbide aggregates. In fact the uniform and total elongation values for martensite starting structures are higher than that obtained using ferrite-carbide aggregates. So definitely, martensite

starting structures seem to be a potential processing route to produce UFG DP steels. But the limitations for using this route is the difficulty in creating the martensite phase in the first place which require very high cooling rate.

Mn content also plays a key role in the processing of DP steels as it substantially enhances the grain size stability during intercritical annealing and the ability of austenite to undergo martensitic phase transformation [65]. This implies that a critical amount of Mn content has to be present in steels otherwise high heating rates (to promote grain size stability) and high cooling rates (to promote austenite to martensite transformation) have to be employed to achieve UFG DP steels. This explains the reason behind the high heating and cooling rates employed by Azizi-Alizamini et al. [7], because the Mn content in their steel was only 0.74 wt pct as compared to the other UFG DP steels, which have at least 1.5 wt pct Mn.

One more important aspect is the distribution of the respective phases (martensite and ferrite). Literature data seems to suggest that a homogeneous distribution of the phases is necessary for achieving promising mechanical properties, but the current study demonstrates that this is not quite necessary. Even in cases of a non-homogeneous size distribution of the phases the mechanical properties of the 0.12 C UFG DP steel displayed a significant improvement compared to those of CG DP steels.

During stamping operation, hole expansion ratio becomes an important parameter that is primarily affected by the fracture behaviour. Here, conventional ferrite-martensite DP steels tend to show inferior behaviour as they are prone to brittle fracture and this has been a major disadvantage for this class of advanced high strength steels. Thus improved fracture properties play a significant role in the selection of DP steels. Plots of UTS vs. fracture strain and strength-

elongation balance (UTS×UE) vs. fracture strain for DP steels with martensite ranging between 15-35 wt pct are shown in Figure 6-2 and Figure 6-3, respectively.

Interestingly, for a given value of UTS, the fracture strain for the UFG DP steels (this study and also from literature) is higher compared to CG DP steels. Decreasing the carbon content seems to help in increasing the fracture strain values as well. The difference in the UTS values of the UFG DP steels from literature and from this study has already been explained. All the DP steels seem to have fracture strain below 1, except for the 0.06C steel, which show a significant improvement in the fracture strain values. One of the possible reasons might be the presence of lower carbon level. Secondly, the martensite content present in these steels is lower compared to others. Also by using low cooling rates during quenching, the martensite tends to temper and becomes more ductile.

In the strength-elongation balance (UTS×UE) vs. fracture strain graph (see Figure 6-3), an envelope is used to separate the CG and UFG DP steels from the literature and the UFG DP steels created in this work. The UFG and coarse grain DP structures from the literature are scattered without following any pattern, although there seems to be a linear relationship between the fracture strain and strength-elongation balance. For a give fracture strain, the strength-elongation balance is higher for the 0.12C steel as compared to coarse and UFG DP steels from literature. Similar to the graph shown in Figure 6-2, here also the 0.06C steel falls in the extreme right of the graph and the reasons might be similar to what has been explained in the previous paragraph.

So overall the 0.12C steel have good UTS and UE balance (comparable to other UFG DP steels), combined with higher strength-elongation and fracture strain values as compared to other UFG DP steels. The 0.06C steel has lower UTS and UE values than all the other UFG DP steels

provided. Although there is one peculiar aspect that can be observed for the 0.06C steel, i.e. the relatively high strain to fracture values compared to other DP steels.

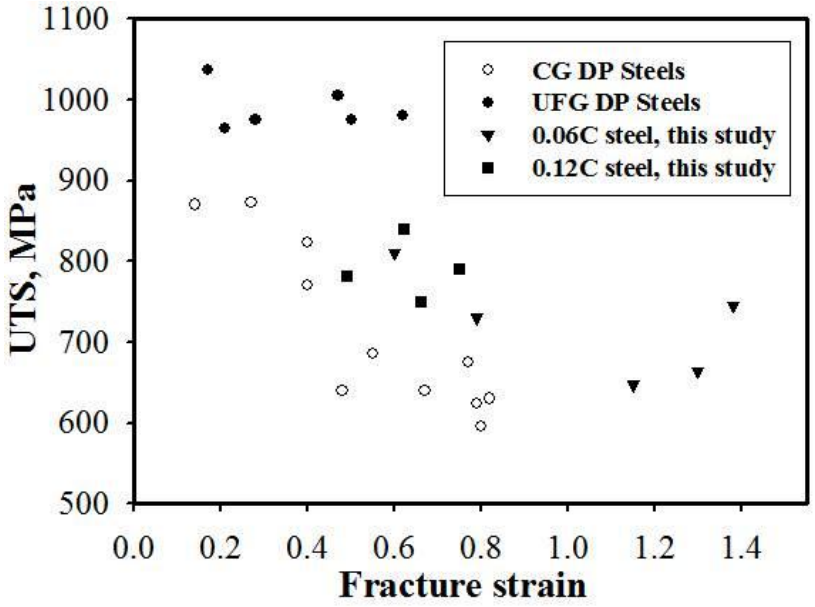

Figure 6-2: Comparison of UTS vs. fracture strain for various DP steels [5, 7, 9, 10, 21, 39, 59, 61, 64].

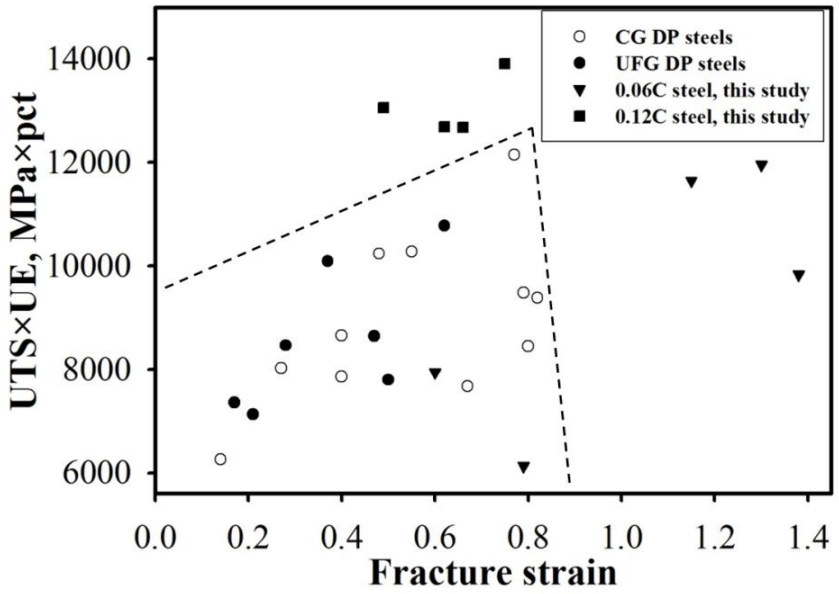

Figure 6-3: Comparison of UTS×UE vs. fracture strain for various DP steels [5, 7, 9, 10, 21, 39, 59, 61, 64].

6.2 Micro-alloyed steels

Nb is generally used as a microalloying addition to obtain grain refinement in steels [66], but on the other hand presence of Nb has significant impact on the recrystallization kinetics. It effectively retards rectystallization because of solute dragging and dynamic precipitate pinning [66, 67]. Nb addition has a greater effect on recrystallization as compared to Mo [68, 69]. Mn also retards recrystallization but has lower effect as compared to Nb and Mo. Solute drag analysis of the effects of the three main alloying elements (Mo, Nb, Mn) indicates that Mo is more effective in retarding grain boundary motion than Mn and that Nb is more effective than Mo when all of these elements are in solid solution [69]. Huang et al. [63] performed a series of annealing experiments to characterize the recrystallization behaviour of plain C-Mn steel with respect to C-Mn-Mo steel. They found that the activation energy for recrystallization has increased by 40% when adding 0.16 wt pct Mo. They also found that the rate of recrystallization was slower in the C-Mn-Mo steel as compared to plain C-Mn steel. The retardation of recrystallization by Mo and Nb may provide an explanantion of why it was impossible in this study to create recrystallized fine ferrite-carbide aggregates in Nb and Mo treated steels. Using martensite as the starting structure for intercritical annealing rather than ferrite-carbide aggregates should be further explored for these microalloyed steels as this would eliminate the recrystallization step.

Very few studies have been reported on fine grained micro-alloyed DP steels (refer chapter 2). The few studies published suggest that their strength and elongation values are lower compared to the UFG DP steels (0.12C) created in this study. In summary, it can be said that alloying additions assist in reducing the heating and cooling rates necessary for processing DP steels,

hence further work should be done to develop new processing routes to achieve UFG DP steels with little alloying additions.

7 Conclusions

In this thesis, the effect of carbon composition and processing parameters on microstructure evolution and mechanical properties in 0.06C and 0.12C steels were studied.

Based on the results obtained, the following conclusions can be made:

(1) Slight modifications in terms of tempering time are necessary for the processing of ferrite-carbide aggregates so as to accommodate steels with varying carbon contents.

(2) For the ferrite-carbide initial structures, lower heating (10 and 100^{o}C/s) and cooling rates (below 300^{o}C/s) are sufficient to obtain UFG DP steels with higher Mn content.

(3) For the martensite starting structures, UFG DP structures are being obtained even for very low heating (1^{o}C/s) and cooling (below 150^{o}C/s) rates. Thus, processing via this route can be used to reduce the processing steps compared to fine ferrite-carbide aggregate.

(4) The 0.06C steel has inferior UTS and elongation balance compared to that of the 0.12C steel. This finding suggest a critical carbon content that is necessary to obtain a good balance of UTS-UE in UFG DP steels.

(5) For the 0.06C steel, employing lower cooling rates for ferrite-carbide initial structures results in considerable improvement in the fracture strain and a similar behavior is obtained for the martensite starting structures.

(6) For the 0.12C steel, with ferrite-carbide starting structures, the balance of mechanical properties are comparable to those of the UFG DP steels from the literature even with lower heating rates (10^{o}C/s). For the martensite starting structures, promising results are obtained even for 1^{o}C/s heating rate.

(7) The strength-elongation balance of UFG DP steels (0.12C) is superior to that of the CG steels from the literature.

(8) The inhomogeneity of the microstructure does not seem to have a detrimental effect on the mechanical properties of the DP steels analysed in this study.

(9) Development of UFG DP steels in micro-alloyed steels remains challenging. Forming fine ferrite-carbide aggregates is rather complicated compared to plain C-Mn steels. Starting with a martensite microstructure seems to be an alternative option instead of ferrite-carbide aggregates.

The following suggestions can be made for future work:

(1) To use martensite starting structures for micro-alloyed steels for fabricating UFG DP steels.

(2) To study the austenite formation behavior upon heating for martensite starting structures.

(3) To perform an in depth analysis for the reason behind the huge strain to fracture values obtained for the 0.06C steel.

(4) To fabricate coarse grained DP steels for both the 0.06C and the 0.12C steels and compare their mechanical properties with the UFG DP steels.

Bibliography

1. "National Highway Traffic Safety Administration", DOT HS 810 863, 2007, <www.nhtsa.gov>.
2. "Euro NCAP", 1998, <http://www.euroncap.com/files/Development-of-Euro-NCAP-1998---0-7498ffa2-36b6-4328-8b6e-f44fe5d35563.pdf>.
3. Fekete, J.R., Hall, J. N., Meuleman, D. J., AIST, 2008, pp. 249-256.
4. "Boron Extrication", 2009, <http://boronextrication.com/2009/08/2009-xc60-body-structure/>.
5. Park, K.-T., Han, S.Y., Ahn, B.D., Shin, D.H., Lee, Y.K., Um, K.K., Scr. Mater., 2004, 51, pp. 909-913.
6. Song, R., Ponge, D., Raabe, D., Kaspar, R., Acta Mater., 2005, 53, pp. 845-858.
7. Azizi-Alizamini, H., Militzer, M., Poole, W. J., ISIJ, 2011, 51, pp. 958-964.
8. Krauss, G., Mater. Sci. Eng. A, 1999, 273, pp. 40-57.
9. Speich, G.R., Miller, R.L., TMS-AIME, 1979, pp. 145-182.
10. Vander Arend, P.J., Rigsbee, J.M., TMS-AIME, 1979, pp. 56-86.
11. Speich, G.R., TMS-AIME, 1981, pp. 3-45.
12. Balliger, N.K., Gladman, T., Met. Sci., 1981, 15, pp. 95-108.
13. Kot, R.A., Bramfitt, B. L., TMS-AIME, 1981, pp. 3-45.
14. Kot, R.A., Morris, J. W., TMS-AIME, 1979, pp. 91-117.
15. Llewellyn, D.T., Hillis, D. J., Ironmaking & Steelmaking, 1996, 23, pp. 471-478.
16. Thomas, G., Koo., J. Y., TMS-AIME, 1979, pp. 183-201.
17. Davies, R.G., Met. Trans. A, 1978, 9, pp. 671-679.

18. Pickering, F.B., Physical Metallurgy and the Design of Steels, Applied science publishers, London, 1978.

19. Klaar, H.J., El-Sesy, I. A., Hussein, A. H. A., Steel Res., 1990, 61, pp. 85-92.

20. Waterschoot, T., De Cooman, B.C., Vanderschueren, D., Ironmaking & Steelmaking, 2001, 28, pp. 185-190.

21. Mazinani, M., Poole, W.J., Met. Trans. A, 2007, 38A, pp. 328-339.

22. Cribb, W.R., Rigsbee, J. M., TMS-AIME, 1979, pp. 91-117.

23. Ashby, M.F., Philos. Mag., 1970, 21, pp. 399-424.

24. Fleck, N.A., Muller, G. M., Ashby, M. F., Hutchinson, J. W., Acta Mater., 1994, 42, pp. 475-487.

25. Bourell, D.L., Rizk, A., Acta Mater., 1983, 31, pp. 609-617.

26. Crawley, A.F., Shehata, M. T., TMS-AIME, 1981, pp. 181-197.

27. Sherman, A.M., Davies, R. G., Donlon, W. T., TMS-AIME, 1981, pp. 85-94.

28. Sakaki, T., Sugimoto, K., Fukuzato, T., Acta Mater., 1983, 31, pp. 1737-1746.

29. Sarosiek, A.M., Owen, W. S., Mat. Sci. and Eng. A, 1984, 66, pp. 13-34.

30. Liedl, U., Traint, S., Werner, E. A., Comput. Mater. Sci., 2002, 25, pp. 122-128.

31. Chang, P.-H., Preban, A. G., Acta Mater., 1985, 33, pp. 897-903.

32. Sakaki, T., Sugimoto, K., Fukuzato, T., Strength of Metals and Alloys, 1982, 1, pp. 455-460.

33. Gerbase, L., Embury, J. D., Hobbs, R. M., TMS-AIME, 1979, pp. 118-144.

34. Davies, R.G., Magee, C. L., TMS-AIME, 1979, pp. 1-19.

35. Hillert, M., Jerkontorets Annaler, 1957, 141, pp. 67-89.

36. Ashby, M.F., Elsevier, London, 1971, pp. 137-192.

37. Anand, L., Gurland, J., Acta Mater., 1978, 24, pp. 901-909.

38. Miller, R.L., Met. Trans. A, 1972, 24, pp. 905-912.

39. Ramos, L.F., Matlock, D.K., Krauss, G., Met. Trans. A, 1979, 10, pp. 259-261.

40. Pickering, F.B., The Metals Society, 1981, pp. 5-25.

41. Shen, H.P., Lei, T. C., Advances in Fracture Research, 1984, 2, pp. 1271-1278.

42. Jardim, O.R., Longo, W.P., Chawla, K.K., Metallography, 1984, 17, pp. 123-130.

43. Steinbrunner, D.L., Matlock, D.K., Krauss, G., Met. Trans. A, 1988, 19, pp. 579-589.

44. Ahmad, E., Manzoor, T., Ali, K. L., Akhter, J. I., Mater. Eng. and Perf., 2000, 9, pp. 306-310.

45. Chawla, K.K., Rios, P. R., Guimaraes, J. R. C., Mater. Sci. Let., 1983, 2, pp. 94-98.

46. Sidjanin, L., Miyasato, S., Mater. Sci. and Tech., 1989, 5, pp. 1200-1206.

47. Sarwar, M., Priestner, R., Mater. Sci., 1996, 31, pp. 2091-2095.

48. Su, Y.L., Gurland, J., Mater. Sci. and Eng., 1987, 95, pp. 151-165.

49. Marder, A.R., Met. Trans. A, 1982, 13, pp. 85-92.

50. Kim, N.J., Thomas, G., Met. Trans. A, 1981, 12, pp. 483-489.

51. Bayram, A., Uguz, A., Ula, M., Materials Characterization, 1999, 43, pp. 259-269.

52. Balliger, N.K., The Metals Society, 1982, pp. 73-83.

53. Samuel, F.H., ISIJ, 1983, 23, pp. 357-360.

54. Leslie, W.C., The Physical Metallurgy of Steels, McGraw Hill, New York, 1981.

55. Terao, N., Cauwe, B., Mater. Sci., 1988, 23, pp. 1769-1778.

56. Tsipouridis, P., Werner, E., Krempaszky, C., Tragl, E., Steel Res. Int., 2006, 77, pp. 654-667.

57. Segal, V.M., Reznikov, V.I., Drobyshevsky, A.E., Kopylov, V.I., Russian Metallurgy, 1981, pp. 99-105.

58. Shin, D.H., Kim, B.C., Park, K.-T., Choo, W.Y., Acta Mater., 2000, 48, pp. 3245-3252.

59. Park, K.T., Y.K. Lee, D.H. Shin, ISIJ, 2005, 45, pp. 750-755.

60. Mukherjee, K., Hazra, S.S., Militzer, M., Met. Trans. A, 2009, 40A, pp. 2145-2159.

61. Calcagnotto, M., Adachi, Y., Ponge, D., Raabe, D., Acta Mater., 2011, 59, pp. 658-670.

62. Calcagnotto, M., Ponge, D., Raabe, D., Mat. Sci. and Eng., 2010, 527, pp. 7832-7840.

63. Huang, J., Poole, W.J., Militzer, M., Met. Trans. A, 2004, 35A, pp. 3363-3375.

64. Calcagnotto, M., Ponge, D., Raabe, D., ISIJ, 2008, 48, pp. 1096-1101.

65. Calcagnotto, M., Ponge, D., Raabe, D., Met. Trans. A, 2012, 43, pp. 37-46.

66. Ma, L.-Q., Liu, Z-Y., Jiao, S-H., Yuan, X-Q., Wu, D, Iron and Steel Res. Int., 2008, 15, pp. 31-36.

67. Kliber, J., Schindler, I., Mater. Proc. Tech., 1996, 60, pp. 597-602.

68. Akben, M.G., Bacroix, B., Jonas, J.J., Acta Metallurgica, 1983, 31, pp. 161-174.

69. Simielli, E.A., Yue, S., Jonas, J.J., Met. Trans. A, 1992, 23, pp. 597-608.